

Diurnal, synoptic and seasonal variability of atmospheric CO₂ in the Paris megacity area

5 Irène Xueref-Remy^{1*}, Elsa Dieudonné^{1,2}, Cyrille Vuillemin^{1,3}, Morgan Lopez^{1,4}, Christine Lac⁵, Martina Schmidt^{1,6}, Marc Delmotte¹, Frédéric Chevallier¹, François Ravetta⁷, Olivier Perrussel⁹, Philippe Ciais¹, François-Marie Bréon¹, Grégoire Broquet¹, Michel Ramonet¹, T. Gerard Spain⁸ and Christophe Ampe⁹

¹Laboratoire des Sciences du Climat et de l'Environnement (LSCE), Gif-sur-Yvette, France

²Now at Laboratoire de Physico-chimie de l'Atmosphère (LPA), Dunkerque, France

10 ³Now at European Organization for Nuclear Research (CERN), Meyrin, Switzerland

⁴Now at Environment Canada, Climate Research Division, Toronto, Ontario, Canada

⁵Centre National de la Recherche Météorologique (CNRM-GAME), Toulouse, France

⁶Now at Institute of Environmental Physics (IEP), Heidelberg, Germany

⁷Laboratoire Atmosphères, Milieux, Observations Spatiales (LATMOS), Guyancourt, France

15 ⁸National University of Ireland (NUI), Galway, Ireland

⁹Association de Surveillance de la Qualité de l'Air en Île-de-France (AIRPARIF), Paris, France

Correspondence to: Irène Xueref-Remy (irene.remy-xueref@univ-amu.fr)

* Now at : OSU Pytheas /University of Aix-Marseille, Marseille, France

Abstract. Most of the global fossil fuel CO₂ emissions arise out of urbanized and industrialized areas. Bottom-up inventories
20 quantify them but with large uncertainties. In 2010-2011, the first atmospheric in-situ CO₂ measurement network for Paris, the capital of France, has been operated with the aim of monitoring the regional atmospheric impact of the emissions coming from this megacity. Five stations sampled air along a northeast-southwest axis that corresponds to the direction of the dominant winds. Two stations are classified as rural (TRN and MON), two are peri-urban (GON and GIF) and one is urban (EIF, located on top of the Eiffel tower). In this study, we analyze the diurnal, synoptic and seasonal variability of the in-situ
25 CO₂ measurements over nearly one year (8 August 2010–13 July 2011). We compare these datasets with remote CO₂ measurements made at Mace Head (MHD) on the Atlantic coast of Ireland, and support our analysis with atmospheric boundary layer height (ABLH) observations made in the centre of Paris and with both modeled and observed meteorological fields. The average hourly CO₂ diurnal cycles observed at the regional stations are mostly driven by the CO₂ biospheric cycle, the ABLH cycle, and the proximity to urban CO₂ emissions. Differences of several $\mu\text{mol}\cdot\text{mol}^{-1}$ (ppm) can be observed
30 from one regional site to the other. The more the site is surrounded by urban sources (mostly residential and commercial heating, and traffic), the more the CO₂ concentration is elevated, as is the associated variability which reflects the variability of the urban sources. Furthermore, two sites with inlets high above ground level (EIF and TRN) show a phase shift of the CO₂ diurnal cycle of a few hours compared to lower sites due to a strong coupling with the boundary layer diurnal cycle. As

a consequence, the existence of a CO₂ vertical gradient above Paris can be inferred, whose amplitude depends on the time of the day and on the season, ranging from a few tenths of ppm during daytime to several ppm during nighttime. The CO₂ seasonal cycle inferred from monthly means at our regional sites are driven by the biospheric and anthropogenic CO₂ flux seasonal cycles, by the ABLH seasonal cycle and also by synoptic variations. Enhancements of several ppm are observed at peri-urban stations compared to rural ones, mostly from the influence of urban emissions that are in the footprint of the peri-urban station. The seasonal cycle observed at the urban station (EIF) is specific and very sensitive to the ABLH cycle. At both the diurnal and the seasonal scales, noticeable differences of several ppm are observed between the measurements made at regional rural stations and the remote measurements made at MHD, that are shown not to define background concentrations appropriately for quantifying the regional (~100 km) atmospheric impact of urban CO₂ emissions. For wind speeds less than 3 m s⁻¹, the accumulation of local CO₂ emissions in the urban atmosphere forms a dome of several tens of ppm at the peri-urban stations, mostly under the influence of relatively local emissions including those from the Charles-De-Gaulle (CDG) airport facility and from aircraft in flight. When wind speed increases, ventilation transforms the CO₂ dome into a plume. Higher CO₂ background concentrations of several ppm are advected from the remote Benelux-Ruhr and London regions, impacting concentrations at the five stations of the network even at wind speeds higher than 9 m s⁻¹. For wind speeds ranging between 3 and 8 m s⁻¹, the impact of Paris emissions can be detected in the peri-urban stations when they are downwind of the city, while the rural stations often seem disconnected from the city emission plume. As a conclusion, our study highlights a high sensitivity of the stations to wind speed and direction, to their distance from the city, but also to the ABLH cycle depending on their elevation. We learn some lessons regarding the design of an urban CO₂ network : 1/ careful attention should be paid to properly setting regional (~100 km) background sites that will be representative of the different wind sectors; 2/ the downwind stations should as much as possible be positioned symmetrically in relation to the city centre, at the peri-urban/rural border; 3/ the stations should be installed at ventilated sites (away from strong local sources) and the air inlet set-up above the building or biospheric canopy layer, whichever is the greatest; and 4/ high resolution wind information should be available with the CO₂ measurements.

Keywords: Carbon dioxide, CO₂ urban plume, anthropogenic emissions, variability, boundary layer height, wind, turbulence, fossil fuel, biospheric fluxes.

1 Introduction

Urbanized and industrialized areas are estimated to produce more than 70% of the global CO₂ emissions based on the consumption of fossil fuels (IEA, 2008, Seto and Dhakal, 2014). Furthermore, due to increased urbanization especially in developing countries, urban CO₂ emissions are projected to grow rapidly in the next decades (e.g. Wolf et al., 2011). Understanding the contribution of cities to climate change will help stakeholders to become active at the city level in taking

proper decisions regarding CO₂ emissions reduction (United Nations, 2011a). Megacities especially are places where human activities release large quantities of CO₂ in the atmosphere and they require scientific and political interest (Rosenzweig et al., 2010; Duren and Miller, 2012).

Based on the 2010 population census, the Paris metropolitan area has 10.5 million inhabitants and is ranked 21st megacity in the world and 2nd in Europe after Moscow (United Nations, 2011b). Paris is centered in the region Île-de-France (IdF) that contains 18% of the French population (INSEE, 2012) while covering only 2% of the territory. The emission inventory reported by AIRPARIF (Association de surveillance de la qualité de l'air en IDF: <http://www.airparif.asso.fr>) estimates that IdF emitted a total of 41.9 Mt of CO₂ in 2010, i.e. 12% of French anthropogenic CO₂ emissions (source: CITEPA, 2012, www.statistiques.dvpt-durable.gouv.fr). It is based on the combination of benchmark emission factors and activity data for about 80 emission sectors and delivered every year (3 years after the year of the emissions reporting). It is built at a high spatio-temporal resolution (1x1 km², 1 h) for the whole IdF domain. The temporal resolution is based on the interpolation of mean hourly diurnal cycles of emissions constructed for 5 typical months (January, April, July, August and October). Detailed information can be found in Bréon et al (2015). However, there is no independent assessment of the regional CO₂ emission estimates given by the AIRPARIF inventory,. The associated uncertainties are estimated to be 20% of the total CO₂ emitted by month, but they are also sector dependent and can reach several tens of percent for some sectors, as also discussed in Rayner et al. (2010).

In the recent years, there has been a growing international interest in quantifying urban CO₂ fluxes from atmospheric top-down approaches (e.g. Duren and Miller, 2012; Mc Kain et al., 2012). Large projects developed in Indianapolis (Influx: <http://influx.psu.edu> ; e.g. Turnbull et al, 2015 ; Lauvaux et al, 2015), Boston (<http://www.bu.edu/today/2013/the-climate-crisis-measuring-boston-carbon-metabolism/> ; McKain et al, 2012), Los Angeles (Megacities: <http://megacities.jpl.nasa.gov/portal/> ; e.g. Newman et al, 2013 ; Verhulst et al, 2016) and in our case Paris (CO₂-Megaparis: <http://co2-megaparis.lsce.ipsl.fr> ; e.g. Lac et al, 2013 ; Bréon et al, 2015 ; Ammoura et al, 2016 ; Staufer et al, 2016). These projects rely on the development of urban atmospheric in-situ CO₂ monitoring networks that should ideally include, all along the dominant wind paths: 1/ regional stations upwind of the city to characterize the regional background CO₂ dry air mole fraction (i.e. without having the impact of the regional emissions - regional is here defined within a radius of ~100 km around the center of Paris); and 2/ regional stations in the city and downwind of it (that will integrate both the background signal and the peri-urban/urban ones). In the following, the term dry air mole fraction is simplified by concentration and is expressed in the part per million (ppm) unit.

Several studies highlighted the fact that the CO₂ concentration measured in and around cities are directly sensitive to factors that control the CO₂ fluxes: proximity to urban centers and industrial sources, ground and air traffic, vegetation distribution, and rates of primary productivity (e.g. Wentz et al., 2002; Apadula et al., 2003; Nasrallah et al., 2003; Gratani and Varone, 2005; Strong et al., 2011). Furthermore, advection and vertical mixing strongly influences the urban CO₂ signal (e.g. Idso et al., 2002; Moriwaki et al., 2006). At low wind speeds, urban CO₂ emissions that accumulate over the city were observed to generate a CO₂ urban dome of several tens of ppm at night and several ppm in the afternoon compared to surrounding rural

areas, reaching for example 100 ppm in Phoenix, Arizona just before pre-dawn (Idso et al., 1998, 2001). At higher wind speeds, the strength of the CO₂ urban dome decreases through ventilation processes to take the shape of a plume, and is considered in some former studies for other cities to reach an asymptotic value (e.g. Rice et al., 2011) which was sometimes considered representative of the regional background CO₂ concentration (Garcia et al., 2012; Massen and Beck, 2011).

5 In the Paris region, no continuous atmospheric CO₂ observation network existed before the present study, apart a couple of intensive campaigns: 1/ Widory and Javoy (2003) performed CO₂ measurements very close to the ground level (mostly under the influence of car exhausts) that we think is not representative of the urban scale; and 2/ in winter 2010, Lopez et al (2013) showed an increase of several ppm in the atmospheric CO₂ concentration in Paris (30 m above ground level, AGL) in comparison with the CO₂ levels measured in the Gif-sur-Yvette station (GIF, 12 m AGL), located in a remote peri-urban area
10 ~20 km SW of Paris. Furthermore, the Mace Head station (MHD - west coast of Ireland) is generally used as the reference site for European CO₂ background measurement (Bousquet et al. 1996), as it has been the case in the Heidelberg (Germany) study of Vogel et al. (2010) or in the Paris study of Lopez et al. (2013). The relevance of this remote coastal site as a regional background site, especially for studying the regional impact of the Paris megacity on atmospheric CO₂ remains to be assessed at the diurnal to the seasonal scales as no regional in-situ network measurements were available to tackle this
15 question.

In the framework of the CO₂-Megaparis project, we deployed a network of in-situ CO₂ stations along the path of the dominant winds and developed high-resolution top-down modeling frameworks dedicated to study the Paris CO₂ emissions (Lac et al., 2013; Bréon et al., 2015). Our observation network consisted of three new continuous sites installed in and around the Paris megacity, among which one on top of the Eiffel tower (317 m AGL). These three stations (named MON,
20 GON and EIF) were deployed in summer 2010 within the AIRPARIF infrastructure. They ran for several months of the CO₂-Megaparis project lifetime and delivered almost one year of CO₂ concentration datasets for the Paris megacity area. Additional datasets were provided by two long-term stations operated by LSCE named TRN (Schmidt et al., 2014) and GIF (Lopez et al., 2012) that are part of the national monitoring network SO-RAMCES (now called ICOS-Fance: <https://icos-atc.lsce.ipsl.fr/>). All the sites are on the same calibration scale (WMO 2007), use similar analytical procedures and have
25 relatively small uncertainties, as we will further explain in details.

This work aims to understand the diurnal, synoptic and seasonal variability of the atmospheric CO₂ concentration observed at each of the five stations of the Paris megacity network from the analysis of the first ~1-year long time series (8 August 2010 - 13 July 2011). We also compare the regional CO₂ concentration datasets to those at MHD ones in order to assess how relevant this remote site is in defining the CO₂ background level in the Paris region. Section 2 introduces the observation
30 network and reports the data treatment and the quality of the CO₂ time series. We also present the meteorological fields used over the period of study as well as observations of the atmospheric boundary layer (ABL) height, collected at the QUALAIR site (QUA) in the centre of Paris, that cover a large part of the period of study (8 August 2010 – 31 March 2011). In section 3, we present air mass back trajectories and the different wind sectors covered to assess the variability of the time series over the year of study (section 3.1). We then analyze the diurnal variations of the CO₂ concentration at the 5 sites that we compare

to the MHD record (section 3.2). A specific focused analysis is carried out on the case of the Eiffel tower station. We also estimate the weekday versus weekend variability (section 3.3) and analyze the seasonal variations of the CO₂ concentration at each site (section 3.4). Finally, we study the role of wind speed and direction on the CO₂ signal collected at the five regional network stations (section 3.5) and we assess the impact of local (<10 km), regional (10-100 km) and remote (> 100 km) fluxes on the observed CO₂ concentrations. We come to conclusions on the representativeness of each site for assessing how the Paris CO₂ emissions impact the atmospheric CO₂ concentration at the regional scale, and on the lessons learned for regional urban network design.

2 Experimentals

2.1 The measurement network

10 2.1.1 Geography of IdF and CO₂ emissions from the Paris region and Western Europe

Paris is located in the region of IdF in a relatively flat area and benefits from a temperate climate, with frequent rain events in all seasons and changing weather conditions. IdF covers 12011 km² i.e. only 2.2% of the national territory. In 2010, land usage was 47% by agriculture, 31% by forests and natural areas and 22% by urbanized areas (http://www.insee.fr/fr/themes/tableau.asp?reg_id=20&ref_id=tertc01201), the last sector increasing in recent decades (United Nations, 2011b). In 2010, anthropogenic CO₂ emissions of IdF came from the residential and commercial buildings (43%), road traffic (29%), industry and energy production (14%), agriculture (5%), waste (4%), aircraft (0-915 m ASL) and airport infrastructures (4%) and worksites (1%) (AIRPARIF, 2010). The CDG airport (relatively close to GON, see below) represents about 78% of the aircraft and airport CO₂ emissions in IDF, with ~60% emitted from airplane traffic on the tarmac and in flight (below 915 m ASL) (ADP, 2013; AIRPARIF, 2013). The Orly airport (16 km east of GIF) emits ~27% of the CDG airport CO₂ emissions (AIRPARIF, 2013). Le Bourget airport (close to GON, see below) CO₂ emissions are much smaller (~1.6% of the CDG one, AIRPARIF, 2013).

Figure 1 shows the total annual CO₂ emissions emitted from IdF at the resolution of 1x1 km² (AIRPARIF, 2010). As shown on Fig. 1, there is a large spatial variability of CO₂ emissions in IdF which is mainly driven by the population density and the location of highways. Each year, average emissions in the center of Paris are estimated to be ~70 000 tCO₂ km⁻² compared to ~5000 tCO₂ km⁻² at the suburban borders. Emissions have a temporal variability on diurnal, synoptic and seasonal scales, mainly because CO₂ emitted by heating varies with temperature and season, and CO₂ emitted by traffic changes with the time of the day, day of the week and vacation periods (see Fig.3, Bréon et al, 2015). Figure 1 also shows emissions from the industry and energy production, that come from point sources here distributed on 1x1 km gridcells. According to AIRPARIF, these sources are located mostly in the north and north-eastern areas of Paris compared with the southern part of Paris (Lopez et al, 2013). Detailed and public information on a total of one hundred and twenty three point sources of CO₂ in IdF can be found online for the year 2010 at the following address: <http://www.georisques.gouv.fr/dossiers/irep/form-etablissement/resultats?annee=2010®ion=11&polluant=131#/>. Some of these point sources are located within a few

kilometers of the sampling sites as detailed in section 2.1.2 and may have an impact on the observed CO₂ concentration, as discussed in section 3.5.2. Figure 2 shows the distribution of fossil fuel and cement CO₂ emissions in Western Europe extracted from the EDGAR v4.0 emission inventory (<http://edgar.jrc.ec.europa.eu/>, 2009), highlighting large anthropogenic emissions spots in the Paris megacity, but also in the Benelux area, the Ruhr valley and the London megacity that may enrich the synoptic air masses with high CO₂ concentrations before they reach the Paris region.

2.1.2 Sampling sites

The location of the observation sites are represented on Fig. 1 and Fig. 2. Table 1 gives their exact geographical coordinates. The sites were carefully chosen so that they would not contaminate the CO₂ measurements by their own emissions.

The Eiffel tower station (EIF) was installed on the highest floor accessible to tourists, in a closed room of 1.5 m² under the stairs providing access to the Tower communication antennas. To prevent contamination by the visitors' respiration, the air inlet was elevated to about 15 m above the last floor accessible to tourists, at the antenna level (317m AGL), where it was protected from uplifted air by several intermediate metallic floors. The instrument was set-up into a Faraday cage to avoid interferences from strong electromagnetic radiations from the antennae. The location of the Eiffel tower is not exactly central within Paris. The 0-180° (N, E and S) wind sector of the station is exposed to a larger urbanized and industrialized area than the 180-270° sector (S to W). In the 0-180° wind sector, the urbanized area covers a radius of about 20 km and includes two large point sources that are the waste burning facility of Ivry (in the SE direction of the Eiffel Tower) and the heating facility of Saint-Ouen (in the North). In the 180-270° wind sector, the urbanized area extends barely within a 10 km radius before entering into broad-leaved trees forests covering ~2300 ha. The 270°-360° wind sector is also mostly urbanized over a radius of about 15 km, although it comprises the woods of Boulogne (about 840 ha) which are located only 2 km NW of the Eiffel tower.

The Gonesse station (GON) was set-up about 20 km north east of the Eiffel tower at the local fire station in a residential area comprising a combination of streets and lawn gardens with a few trees around. The analyzer was hosted in a shelter equipped with a mast of ~4 m standing below the canopy level (~15m AGL). However the distance from the mast to the closest trees was at least 20m and the station was well exposed to wind from all directions. GON is located on a small hill relative to the centre of Paris and in the southerly direction, the station benefits from an open view of the city. About 3 to 4 km to the southeast and east of the station is a highway which carries high traffic during rush hours, as early as 5 am local time. The highway connects the centre of Paris and CDG airport, which is located about 7 km northeast of GON. The station is also close to the Bourget Airport located about 2.5 km to the south. Finally, in the W-NW sector, two noticeable industrial sources located at about 5 km from Gonesse (Fig.1) should be mentioned as they might have an influence on the CO₂ measurements (section 3.5.2) : a thermal plant in Sarcelles that emitted 44 ktCO₂/year in 2010, and an energy production plant in Le Plessis-Gassot that emitted 128 ktCO₂/year in 2010 (source: <http://www.georisques.gouv.fr>).

The Montgé-en-Goële station (MON) was set up in the small village of the same name with approximately 700 inhabitants located on the middle of the slope of a small hill (~20m high). The analyzer was installed on the top of the 3-floor city hall building (~9 m AGL). The air inlet was set-up on an arm pointing about 1.5m outside of the window towards the south (200°) opening onto fields. The north sector was covered by a few houses situated at the edge of a wood of broad-leaved trees. The city hall is located on the southern side of the main road of the village which approximately follows a northwest-southeast axis. Most of its close surroundings are agricultural fields and small villages connected by secondary roads. Montgé-en-Goële is located approximately 10 km east of CDG airport. Two noticeable point sources are relatively close to the station (Fig.1) and could influence the measurements (section 3.5.2) : a cement plant 3 km east in Saint Soupplets (43 ktCO₂/year in 2010, source: <http://www.georisques.gouv.fr/>) and a waste burning facility 7 km east in Monthyon (106 ktCO₂/year in 2011, source: <http://www.georisques.gouv.fr/>). MON was considered as a NE rural site for the Paris megacity.

The Gif-sur-Yvette station (GIF), previously described in Lopez et al (2012) and Lopez et al (2013), has been running continuously since 2001 at LSCE (Laboratoire des Sciences du Climat et de l'Environnement). The air inlet is set up on the roof of a building at 7 m AGL. The site is located ~20 km south-west of the centre of Paris on the Plateau de Saclay and surrounded mainly in the 0°-90° sector by agricultural fields and by a few villages. A few hundred meters further in this direction, a national road passes on a north-south axis with high traffic levels during the morning and in the evening during rush hours. About 1 km further in the 270-360° sector, the atomic and environmental research agency (CEA of Saclay) holds approximately 7000 employees and is equipped with a thermal plant (17 ktCO₂ in 2010, source : <http://www.georisques.gouv.fr/>) and that is further surrounded by agricultural fields. In the last wind sector (90°-270°), a band of forest of about 1 km depth extends along the west to east axis down to the bed of the Yvette river. A noticeable point source in the vicinity of GIF, a thermal plant located in Les Ulis, is located about 5 km further south-east (98.5 ktCO₂ in 2010, source: <http://www.georisques.gouv.fr/>). The GIF station is located roughly at the same distance from the Eiffel tower as GON. However, the environment is more rural in GIF than in GON so that we can label GON as a residential peri-urban site and GIF as a remote peri-urban site - although it is not as rural as the site at MON. Orly airport is located about 16 km east of GIF.

The Traînou station (TRN), previously described by Schmidt et al (2014) has been running continuously since 2007. It is located about 120 km south of the center of Paris in the region "Centre", within the Orleans forest (50000 ha). A 200 m transmitter mast was equipped with four sampling levels: 5 m, 50 m, 100 m and 180 m AGL. TRN is located ~13 km northeast of the city of Orléans which has about 120 000 inhabitants. There are a few villages around the station, including Traînou village with 3195 inhabitants in 2012 (<http://www.insee.fr/fr/themes/comparateur.asp?codgeo=com-45327>). The station is surrounded by agricultural fields and a mixed forest composed of deciduous and evergreen trees. In this study, we use the datasets sampled from the 50m and 180m levels. TRN is considered as a rural site for the Paris megacity.

The Mace Head station (MHD) has already been described by Biraud et al (2000) and Messenger et al (2008). Atmospheric CO₂ has been continuously measured there since 1992. This station, located on the west coast of Ireland, is an important site for atmospheric research in the northern hemisphere, as its remote location facilitates the investigation of trace constituent

changes in marine and continental air masses. Most often, the station receives maritime air masses, although sometimes it is in the footprint of continental air masses coming from Europe, or more locally from Ireland and the UK (see Messenger et al., 2008 for further details). In this study, MHD was evaluated as a potential background site for urban regional studies in the European continent.

- 5 The Qualair station (QUA) is located in the Paris city center on the campus of Université Pierre et Marie Curie in Jussieu on the top floor of a building (25 m AGL), about 4 km east of the Eiffel tower along the Seine river. It is briefly described in Dieudonné et al (2012). This station allows monitoring the height of the urban atmospheric boundary layer (ABL) above the Paris megacity.

2.2 CO₂ measurements

10 2.2.1 Measurement system and calibration procedure

The CO₂ datasets of the CO₂-Megaparis stations (MON, GON and EIF) were collected from 8 August 2010 to 13 July 2011 using CRDS (Cavity Ring Down Spectroscopy) analyzers (Picarro, model G1302) at 0.5 Hz. These three stations were identically setup: atmospheric air was pumped through short inlet lines made of Synflex® (4.3 mm inner diameter) with a flowrate of 0.15 L.min⁻¹. The cell temperature of the analyzers was controlled at 45° C and the cell pressure at 140 Torr. At 15 EIF, the analyzer was specifically designed to undergo higher temperatures inherent to the metallic structure of the tower and the cell temperature set point was set higher (60° C). No specific impact of this set point was observed on the measurements. Air was not dried before analysis at the 3 stations and we applied the automatic CO₂ water correction implemented on the CRDS instruments (Rella, 2010) to our datasets.

The GON and MON stations were equipped with four high pressure aluminum cylinders containing gas mixtures of CO₂ in 20 synthetic air (matrix of N₂, O₂ and Ar) for instrument calibration. Before on-site deployment, the CO₂ concentration of the cylinders was assigned at LSCE on the WMO-X2007 scale by a gas chromatograph (GC) described in Lopez et al (2012). It spanned a range from 370 ppm to 500 ppm. At each site, three of the tanks were used for instrument calibration and measured every 2 weeks. The calibration sequence consisted of four cycles (6 h total). One cycle measured the tanks one after the other for 30 minutes each. The fourth tank called “target” was run for 30 minutes every 12 hours. The target was 25 used to monitor the instrumental drift and to assess the dataset accuracy and repeatability. At EIF, for safety reasons it was not possible to leave any gas tanks on the site so the target tank was measured every two weeks and the calibration gases every 3 months only (two calibration cycles of 20 minutes for each gas, for a total sequence of 2 hours). The instrumentation and the calibration procedure of the two SO-RAMCES stations (GIF and TRN) have already been described in Lopez et al. (2012, 2013) and Schmidt et al (2014).

30 2.2.2 Data processing and quality control

The CRDS CO₂ data were calibrated by applying a linear fit to the CO₂ concentration of the calibration tanks as measured by the CRDS analyzer vs the CO₂ concentration as measured by the GC. Gas equilibrium issues implied retaining only the last calibration cycle of the 4 cycles at MON and GON (and of the 2 cycles at EIF) to compute the calibration equation. For all of the calibration and target gas cylinders, the CRDS CO₂ concentration was calculated as the average of the last 5 minutes of each gas. The accuracy of the datasets was calculated as the mean difference between the CO₂ concentration reported by the CRDS analyzer and by the GC for the target gas. The long-term repeatability of each dataset was calculated as the standard deviation of the mean concentration of the target gas reported by the CRDS analyzer over the year of observations.

Table 2 summarizes the accuracy (≤ 0.13 ppm) and repeatability (≤ 0.38 ppm) calculated from the 5 minute averaged data for MON, GON and EIF. As expected, the dataset of EIF shows larger deviations compared to GON and MON due to less frequent calibration and target gas measurements and a shorter calibration procedure.

The data of GON, EIF and MON were automatically filtered against cavity pressure (P) and cavity temperature (T) departure to the set points (P₀ and T₀) according to the ICOS procedure (Hazan et al, 2016), keeping only points for which $|P-P_0| < 0.1$ Torr and $|T-T_0| < 0.004^\circ$ C for MON and EIF (0.006° C for EIF). Furthermore, dead volumes in the set-up lead to instability in the response of the analyzer for 2 minutes after switching from one gas line to another. These 2 minute periods were automatically removed from the datasets.

The data was also manually inspected to remove CO₂ spikes due to very local influences (e.g. fire training at the GON station, breathing of a maintenance operator on the sampling inlet...). Very local influences were identified from the short duration of the events (a few seconds to some minutes) and from the large standard deviation of the CO₂ averages associated with these events. This amounted to less than 1% of the total datasets, resulting in 91% of the data validated after the (P, T) filtering and the manual quality control.

The GIF, TRN and MHD data processing and quality check were assessed in previous studies by Schmidt et al (2014) and Messenger et al (2008): the repeatability of the 1 h average CO₂ concentration of the target gas is 0.05 ppm at GIF, 0.06 ppm at TRN and 0.05 ppm at MHD. The instrumentation at these 3 sites is directly linked to the WMO-X2007 scale (Zhao et al, 2006).

At each station, some instrument failures occurred during the period of the CO₂-Megaparis study. The amount of available data points in the final datasets which are all provided as hourly averages is reported in Table 3 for each month and for each site, and is in most cases above 80%.

In the following study, we will use CO₂ hourly means for all of the stations. Apart from a few exceptions that will be identified, time is always given in hours UTC. Local time in Paris is UTC+2 from April to October and UTC+1 from November to March.

2.3 Atmospheric boundary layer height measurements

ABL heights over Paris were determined using the 532 nm elastic lidar of the QUALAIR station (<http://qualair.aero.jussieu.fr/>) from 8 August 2010 to 31 March 2011. A description of the instrumental setup and data processing can be found in Dieudonné (2012, 2013). The ABL height (ABLH) can be retrieved from elastic lidar measurements because the lidar signal is proportional to the backscattering coefficient of aerosols. In fair weather, this leads to a sharp signal decrease between the polluted boundary layer (where aerosols emitted from the surface are trapped) and the clean free troposphere. The altitude where the signal first derivative reaches its absolute minimum corresponds to the center of the entrainment zone (Menut et al. 1999). The depth of the layer where the signal first derivative is lower than 80 % of its absolute minimum is used to estimate the base of the entrainment zone, which corresponds here to the lowest ABL height (LBLH) estimate. More complex situations can occur, when elevated layers of aerosols are present in the free troposphere. In that case the absolute minimum of the signal gradient can be located other than at the top of the ABL. To resolve such situations, threshold conditions are applied to discriminate significant minima of the signal gradient (Dieudonné, 2012) and results are manually inspected to check for temporal continuity (as the altitude of a layer cannot vary much from one lidar profile to the next). When the ABL is capped by a cloud, the very strong light scattering by water droplets creates a sharp increase of the lidar signal at the top of the ABL. In such cloudy weather, the cloud base height is the best estimation for the ABLH. The LBLH is calculated as in fair weather.

The ABL height database was constructed by applying this detection method to hourly average lidar data, leading to hourly average ABL depth values. The data were acquired during daytime and weekdays, since an operator had to be on site to shut down the system in case of rain. The dataset covers 70% of the year of study.

2.4 Meteorological fields

Urbanized areas are characterized by specific meteorological patterns (e.g. Masson et al., 2000). For example, the urban heat island effect was observed to generate a gradient of temperature of a few degrees and a gradient in the ABLH of several percent between Paris city center and its rural surroundings (Pal et al, 2012 ; Lac et al, 2013). As far as possible, it is thus appropriate to use local meteorological fields for each of the regional atmospheric CO₂ stations. Since our sites were not equipped with their own meteorological sensors, the Meso-NH model was run over the full period of study at a time step of 60 s and a spatial resolution of 2 km to generate wind speed and direction over a domain including Île-de-France (Lac et al., 2013). This modeling framework includes the land and-surface-atmosphere interaction model SURFEX with an urban scheme (Town Energy Balance (TEB); Masson, 2000) and a vegetation scheme (Interactions between Soil, Biosphere, and Atmosphere (ISBA-A-gs); Calvet et al., 1998; Noilhan and Planton, 1989). It was already validated against observations for one week of March 2011 in Lac et al (2013), where it is described in detail. The meteorological fields were extracted for the present study from the model with an output frequency of 1 h at the sampling height of each station. About 1.5 km north of GIF at the CEA of Saclay (SAC), a mast equipped with meteorological sensors provided wind fields data at 10m AGL from August 2010 to April 2011. In that period, the observed SAC and the modeled GIF meteorological datasets match each other

on average within 0.8 m s^{-1} for wind speed, and 3.7° for wind direction, giving additional confidence in the average behavior of the model, at least in such peri-urban areas.

For wind fields at MHD, we use a local meteorological hourly observation dataset provided by Met Eireann (<http://www.met.ie>).

- 5 Fig. 3 shows the wind roses at GIF for each season (using Meso-NH modeled data), given that the synoptic features are broadly similar to all of the regional stations. Two dominant wind regimes were observed according to the general meteorological features of the region: the southwest regime dominates mostly in summer, autumn and winter, and a northern regime (northeast and northwest sectors) mostly in spring and winter. Wind speed varied from $\sim 0 \text{ m s}^{-1}$ on 18 September 2010 to a maximum of 11.1 m s^{-1} on 13 November 2010, the mean wind speed being 3.4 m s^{-1} . The first (25%) and third
- 10 (75%) quartiles were 2.2 m s^{-1} and 4.4 m s^{-1} , respectively. The main variations of wind speed occurred during changes of synoptic conditions. In MHD, winds blew mostly from the Atlantic Ocean in all seasons, including both the southwest and the southeast sectors. MHD also sometimes received continental air masses mostly in winter, spring and autumn. At this station, wind speeds ranged from 0.1 to 25.3 m s^{-1} with a mean at 7 m s^{-1} and the first and third quartiles at 4.1 and 9.5 m s^{-1} , respectively.
- 15 Regarding temperature, field observations were available over the full period of study at 100 m AGL at SAC (but not closer to the surface). Since we are mostly interested in relative variations of the temperature at the seasonal scale, we use this dataset as a proxy of the air temperature for all stations located in IdF (although we know that the urban heat island can generate differences of a few degrees between the city and its surroundings, as shown in Pal et al., 2012). The hourly temperature dataset collected at SAC 100 m AGL over the whole period of study is shown on Fig. S2. Temperature ranges
- 20 from a minimum monthly mean of 0° C in December to a maximum monthly mean of 18.8° C in August.

3 Results and discussion

3.1 Air mass backtrajectories and wind classification of the CO_2 concentration time series

- In order to get information about the origin of the air masses that reached our stations, back trajectories from the HYSPLIT model (Hybrid Single Particle Lagrangian Integrated Trajectory: http://www.arl.noaa.gov/HYSPLIT_info.php) model were
- 25 calculated for the Paris city over the full period of study. We used wind fields from the NOAA-NCEP/NCAR reanalysis data archives, at a $2.5^\circ \times 2.5^\circ$ and 6 h resolution (<http://rda.ucar.edu/datasets/ds090.0/>). The back trajectories were run for 72 h backwards and started at 10 m AGL. They were then aggregated on monthly plots that are shown in the supplementary material (Fig.S1). In all cases, the monthly clusters illustrate the high variability of the origin of the air masses, which could pass over high CO_2 emissions areas such as the megacity of London, the Benelux or the Ruhr regions before reaching IdF.
- 30 The air masses could also be advected from clean areas such as the Atlantic Ocean, or from biospheric regions such as in the middle of France. This high atmospheric transport variability implies that the Paris regional CO_2 background signal may be highly variable depending on the synoptic conditions and that wind direction and speed are key parameters to take into

account in order to understand the CO₂ concentrations recorded at the different sites. The Hysplit model does not have a sufficient resolution to get a more precise and quantitative information on the influence of local, regional and remote emissions on our CO₂ observations, and getting higher resolved transport information would require a very specific (and expensive) modeling work that is out of the scope of this study. Therefore, in order to go further into the analysis, we used the modeled meteorological fields presented in section 2.4 to classify the CO₂ hourly timeseries into six wind classes (Figure 4a and Figure 4b). The *local class* is defined for wind speed less than 3 m s⁻¹ and the *remote class* for wind speed higher than 9 m s⁻¹. For wind speeds between 3 and 9 m s⁻¹, we defined four remaining classes according to the wind direction: *northeast* (NE), *northwest* (NW), *southeast* (SE) and *southwest* (SW). As an example, in GIF the partition of air masses between the different wind sectors over the full period of study is the following: 16% from the NE, 15% from the NW, 24% from the SW, 7.5% from the SE, 36% from the *local class* and 1.5% from the *remote class*.

On Fig. 4a and Fig. 4b, as expected, wind direction and windspeed appear to be part of the main controlling factors of the CO₂ mixing ratio values recorded in the different stations. The urban and peri-urban stations are characterized by higher mixing ratios and a much larger variability than the rural and background sites. The highest variability is observed on the GON timeseries, followed by EIF and GIF. We note as well that the highest mixing ratios recorded at the southern rural sites (TRN50 and TRN180) and remote station of MHD occur usually during local events, likely from the influence of local emissions, or remote events with northeast winds that passed over Benelux and Ruhr areas (see backtrajectories in S1) and got loaded with anthropogenic emissions (Xueref-Remy et al, 2011) before reaching IdF. We also observe simultaneous variations between the sites for the local wind class: for example peaks of CO₂ mixing ratio are observed in all the stations of IdF in mid February and the end of March 2011, which correspond to two pollution events reported by AIRPARIF (www.airparif.asso.fr). However, there are some other dates (not reported by AIRPARIF as pollution events) during which the CO₂ mixing ratio peaks at the urban and peri-urban stations and also sometimes at the rural stations (ex: 20-25 August and 22-25 October). The wind classification applied on the datasets will be further used to better assess the general features of the CO₂ seasonal cycles, and a much finer wind analysis will be conducted in section 3.5.2 to assess the role of local, regional and remote emissions on the CO₂ timeseries collected within the Paris observation network.

25

3.2 CO₂ diurnal cycles

3.2.1 Mean CO₂ diurnal cycles

Diurnal cycles of atmospheric CO₂ are affected by local sources and sinks, regional transport and ABL dynamics (Fang et al., 2014; Garcia et al., 2012; Rice et al., 2011; Artuso et al., 2009; Gerbig et al., 2006). The mean CO₂ diurnal cycles and associated 1- σ standard deviation are shown in Fig. S3 for the different stations.

Noticeable differences are observed between the sites. The diurnal amplitude of the CO₂ concentration from the lowest to the highest is 2.6 ppm (MHD), 6.5 ppm (TRN180), 11.2 ppm (EIF), 14.9 ppm (MON), 15.5 ppm (TRN50), 18.2 ppm (GIF) and

30.6 ppm (GON). While the CO₂ diurnal pattern at TRN can mostly be explained by biospheric activity and vertical dilution in the ABL (Schmidt et al, 2014), the peri-urban and urban stations are also expected to be strongly influenced by the diurnal cycle of Parisian anthropogenic sources. For all sites except EIF, the maximum concentration occurs in the late night/early morning (4-5 h for TRN50, MON, GIF and GON; 7-8 h for TRN180) when the ABL is the most shallow, vegetation respire
5 and rush hours traffic occurs (5 h - 9 h, source : <http://www.dir.ile-de-france.developpement-durable.gouv.fr/les-comptages-a174.html>). The minimum of the cycle occurs in the afternoon (14 h to 17 h) when the ABL is the deepest and well mixed and during seasons when the vegetation photosynthesis is active. Note that, as for the case of Los Angeles (Newman et al, 2013), the annual mean CO₂ concentration does not peak during rush hours, meaning that traffic is not the primary driver of the shape of the annual CO₂ diurnal cycle at the Paris surface stations, nor are other anthropogenic sources, but rather, the
10 main drivers seem to be the biospheric activity and the ABL dynamics, deadening the diurnal features of anthropogenic emissions. The case of EIF is specific due to its elevation and a strong interaction of urban CO₂ emissions with the ABL cycle (see section 3.2.3). As a consequence, the maximum CO₂ concentration at EIF occurs in the mid-morning (10 h) and its minimum is at night (0 h).

Comparing the 50 and 180 m levels at TRN, we observe a vertical gradient of CO₂ concentration, along with a phase shift of
15 the diurnal cycle: the maximum concentration is observed at 5 h at TRN50 versus 7 h at TRN180, due to the coupling of the CO₂ fluxes with the ABL cycle. CO₂ emitted during the night and early morning by anthropogenic sources and by the biosphere's respiration accumulates near the ground into the shallow nocturnal boundary layer (Schmidt et al., 2014) until the ABL develops in the morning, uplifting CO₂ (from 5 h to 7 h) to the 180m level. In the afternoon, when the ABL is well-mixed and deeper than 180m, the mean difference between the concentration at the 50 and 180 m levels is very low (0.3
20 ppm). Furthermore, as noticed in Schmidt et al (2014), the amplitude of the diurnal cycle decreases with increased sampling height as elevated sampling levels are decoupled from the CO₂ sources during the night. As reported in Fang et al (2014), this covariance between biospheric CO₂ activities and the ABL dynamics can make it difficult for inversion models to properly reproduce the CO₂ vertical gradient and thus, use nighttime data for inversions. During mid-afternoon, the ABL is well mixed and the vertical bias would be very tiny.

25 There is a significant enhancement in the CO₂ concentration observed at the regional stations compared to MHD, that increases the closer a station is to Paris city (apart from EIF). The difference of concentration observed between two sites depends on the time of the day and its variation is mainly driven by the CO₂ diurnal cycle at the continental sites. Apart from EIF, the more the station is surrounded by urbanization, the higher is the concentration enhancement compared to MHD, as the average levels of the CO₂ concentration recorded at a station increases with a higher proximity to anthropogenic
30 emissions from Paris. The left panels (a-g) on Fig. 5 show that the hourly 1- σ variability of the mean diurnal cycle remains quite constant over the day at TRN50, TRN180 and MHD. It is a bit more variable for the rural and remote peri-urban stations that are located within IdF (MON and GIF). The variability changes significantly with the time of the day at EIF and even more at GON. We can conclude that: 1/ the more the station is within the urbanized part of the city, the more variable is the measured CO₂ signal, which reflects the spatial and temporal variability of anthropogenic emissions coupled to

atmospheric transport fluctuations; and 2/ the MHD signal is several ppm below the continental signals, even at the rural site of TRN that has already been shown not to be significantly influenced by the Paris megacity fluxes (Schmidt et al, 2014). Thus, MHD does not reproduce the background diurnal variability observed in the rural stations of IdF, and is clearly not a relevant background site for continental European urban studies at the diurnal scale and at the regional scale of ~100 km.

5 The right panels (a'-g') of Fig. 5 show the mean diurnal cycle at each site by season. The influence of anthropogenic activities on the observed CO₂ concentration is expected to be the highest in wintertime when emissions from heating are superimposed on traffic and other sources, photosynthesis is minimal and the diurnal ABL is thinner. Although they vary with the time of the day, on average CO₂ emissions from traffic are quite constant throughout the year but they vary at the hourly and daily scales (according to the AIRPARIF 2010 inventory : on average, 1.5kt.yr⁻¹ during weekends and 2.5 kt.hr⁻¹ during weekdays, and up to 4 kt.hr⁻¹ during traffic peaks ; see Fig. 4 in Bréon et al, 2015). On the contrary, emissions from gas combustion (from the residential, the public and the commercial infrastructures that include mostly heating, production of hot water, air conditioning and cooking) show a seasonal cycle (mainly from heating), releasing about 2.5 kt.hr⁻¹ of CO₂ in the atmosphere in winter versus approximately 1.5 kt.hr⁻¹ in summer (AIRPARIF, 2010 ; Bréon et al, 2015). The biospheric fluxes show large diurnal and seasonal cycles, as mentioned in Bréon et al (2015) who reported net ecosystem exchange (NEE) outputs from the C-TESSSEL model for the Paris region : NEE values are the highest in spring (-10 to -25 kt.hr⁻¹ during daytime and + 5 kt.hr⁻¹ during nighttime, and a daily mean of -5/-10 kt.yr⁻¹ which is the same order of magnitude as fossil fuel emissions i.e. 7 to 9 kt.hr⁻¹ in spring), a bit lower in summer and autumn and much smaller in winter (-3 kt.hr⁻¹ during daytime and +2 kt.hr⁻¹ during nighttime, and a daily mean of -1 kt.hr⁻¹, which is much smaller than fossil fuel emissions that reach 10 kt.hr⁻¹ in winter). In the Supplementary material S4 ,we give for each site the annual and seasonal averages of the daily minimum and of the daily maximum of the hourly concentration, along with the annual and seasonal averages of the diurnal cycle amplitude (max-min concentration difference). The lines entitled "variation" give the mean of the hourly 1-σ standard deviation of the min and of the max of each diurnal cycle.

It is noticeable that the mean winter concentration is about 6 ppm higher at MON than in TRN50. Both stations are in rural environment, but MON is closer to Paris than TRN. As the signals are quite similar in summer, this difference can not likely be explained by the biospheric activity, and is more probably partly due to a higher anthropogenic influence in MON. However, we need here to take into account the difference of the stations inlet height (9 m AGL at MON, 50 m AGL at TRN50) : as shown in Schmidt et al (2014) for the 2010 winter season at Trainou, during daytime CO₂ concentration measured at 10 m AGL and 50 m AGL are similar, but this is not the case during nighttime when the CO₂ concentration is about 3 ppm higher at 10 m AGL than at 50 m AGL because atmospheric mixing is not existent at night and CO₂ sources accumulate near the surface (Denning et al, 1995). This means that the difference between MON and TRN at the inlet height of MON is of the order of 6 ppm during daytime and twice as low during nighttime. This is consistent with the hypothesis of a higher impact of anthropogenic emissions in MON than in TRN, that according to AIRPARIF are lower during nighttime than during daytime, although we do not observe the same order of magnitude (AIRPARIF gives a ratio of daytime over nighttime emissions equals to 3 to 4 in wintertime, while we observe a ratio of 2 ; see Fig.3 in Bréon et al, 2015). Remember

though that the diurnal cycle of the emissions inventory is an average for the whole IdF region, and not only for the MON area. The impact from local sources and/or the CO₂ emission plume of the Paris megacity on MON will be further inferred from the wind analysis in section 3.5.

5 The influence of urban emissions in GIF, MON and GON results in a higher mean diurnal concentration of atmospheric CO₂ at these sites compared to the others for all seasons (and mainly in winter) and of its variability. The impact of traffic emissions is well visible in GIF, MON and GON in the winter season only with two CO₂ maxima during rush hours (morning and evening). Although traffic occurs throughout the year, these peaks are likely more or less masked by the biospheric activity and the ABLH dynamics during the other seasons (see above). In addition, the ABL is shallower during winter leading to higher CO₂ concentrations. The amplitude of the morning and evening peaks is higher in GON than in GIF and MON and denotes a stronger impact of traffic emissions in GON than in the two other stations. GON also shows the maximum inter seasonal difference between summer and winter (31.3 ppm in the afternoon) which is higher than the mean annual afternoon dispersion, meaning in other terms that the seasonal variability is higher than the mean annual dispersion of the fluxes in the afternoon. Actually, the whole diurnal cycle is shifted towards higher concentrations at GON, the mean concentration being higher in GON than in GIF, TRN50, TRN180 and MHD for all seasons, with the largest differences in winter. The full variability observed at GON over the year can thus be explained partly by the seasonal variation of biospheric activity and ABL dynamics, but also by a strong impact of anthropogenic CO₂ emissions variability. The impact of the Paris emissions vs more local sources around the station (highways, airports, heating, industrial facilities...) will be further assessed in Section 3.5.

3.2.2 The specific case of the top of the Eiffel tower

20 In all seasons, the CO₂ diurnal cycle at EIF is out of phase with the other stations, with a maximum occurring later, in the mid-morning instead of the late night/early morning (Fig. 5 and Fig. S3). EIF is significantly higher (317 m AGL) than TRN180 (180 m AGL) so when comparing these elevated sites to ground stations, the effect of the CO₂ coupling with the ABL dynamics can be expected to appear stronger at EIF than at TRN180. Such coupling was already mentioned in the framework of a direct CO₂ transport modeling study in March 2011 (Lac et al., 2013). Furthermore, Dieudonné et al (2013) demonstrated the existence of a vertical concentration gradient between the bottom and the top of the Eiffel tower for NO₂, a species co-emitted with CO₂ during combustion processes especially by the traffic sector, and this vertical gradient was shown to be correlated with the ABL dynamics.

We show in the supplementary material S5 the hourly means of the LBLH observed at the QUALAIR station during daytime, colored by hour, and compared with the level of the EIF station. These data are summarized in Table 4. We recall that the LBLH dataset does not cover the whole period of study, but the most interesting of it as it includes the cold months during which the LBLH and dynamics are at their lowest. The period of August to March allows us to observe a large portion of the seasonal cycle of the LBLH which is characterized by a change in its maximum value (on average 1200 m in

summer, 400m in winter) and in the phase of its development, which starts earlier in summer. We do not have the proper data to quantify precisely this starting time, however we note that the LBLH is always above the level of EIF in summer, while it is below (at 301m on average) before 6 h in winter (see Table 4). We can thus infer that the EIF station could be often above the nocturnal layer at night, inside the residual layer (but not in the free troposphere).

5 In Fig. 6, we show the CO₂ diurnal cycle for each season computed using only the data that were collected at the EIF station at the same time as the LBLH data. The CO₂ signal increases in the morning when the growing ABL brings to EIF the nighttime and early morning CO₂ emissions that got trapped into the nocturnal and/or nascent boundary layer. However, compared to TRN180, the effect at EIF is much stronger due to larger emissions in the city, especially from the morning traffic peak (from 6 h to 10 h local time i.e. 4-8 h UTC in summer and 5-9 h UTC in winter) [<http://www.dir.ile-de-france.developpement-durable.gouv.fr/les-comptages-a174.html>]. Later, the CO₂ signal dilutes into the growing ABL to reach a minimum in the afternoon.

Autumn. The LBLH is close to the EIF altitude. The moderate development of the ABL during the morning does not compensate for the accumulation of the peak traffic emission in the ABL, so that the CO₂ concentration increases from 5 h to 10 h, leading to a CO₂ increase of 17.1 ppm for an LBLH increase of 470 m. At the end of the afternoon, the LBLH
15 decreases and it gets close to the level of EIF, decoupling the station from the surface. This could explain why the late night/early morning concentrations are relatively low and the morning bump of CO₂ quite large. However this remains an hypothesis as we do not have enough points for a robust demonstration.

Winter. As expected, the process of vertical mixing is quite slow in wintertime. The CO₂ concentration increases in the morning (~ + 6 ppm) with the maximum concentration encountered at 13 h for a development of the LBLH of only ~157 m
20 within a 7 hour time frame. After the morning flush of the surface emissions due to the growth of the ABL, the concentration decreases quite rapidly to reach its daily minimum at 16 h. At the end of the day, the LBLH falls and gets quite rapidly below the EIF station level, decoupling the EIF station from the surface. Although we do not have Lidar data after 18 h to confirm it, this likely explains the relatively low level of CO₂ concentrations observed late at night.

Spring. In spring, the CO₂ signal increases until 10 h to a maximum of 420 ppm while the ABL height increases by ~287 m.
25 The shape of the CO₂ mean concentration and LBLH diurnal cycles suggests that the relatively high CO₂ concentrations encountered in the late night/early morning result from the evening high CO₂ emissions trapped into the previous day ABL that became at night the residual layer.

Summer. The CO₂ concentration is on average lower than in the other seasons due to local and regional photosynthesis activity, lower anthropogenic emissions levels and higher LBLH. In particular, the observed LBLH during daytime is always
30 above the EIF station level (Fig. S5) so that one would expect CO₂ concentrations to peak in phase with the traffic counter records, between 6 h and 7 h. However, the CO₂ diurnal cycle at EIF remains out of phase with those recorded at ground level stations, though the delay with the morning peak is reduced compared to other seasons. The CO₂ concentration remains quite stable between 7 h and 9 h, despite the increasing LBLH (+460m) and the decreasing traffic counts. However, one must keep in mind that until late morning, the air dragged into the ABL by entrainment does not come from the clean free

5 troposphere but from the polluted residual layer, explaining why high CO₂ concentration can maintain. After 9 h, the CO₂ concentration steadily decreases, though the average LBLH still increases. This drop in concentration can be explained both by an increase in the photosynthetic activity with increasing solar flux, and by vertical dilution. Indeed, though the LBLH still rises after 10h, the entrainment zone goes on growing until the mid-afternoon (Dieudonné, 2012) blending in clean air from the free troposphere. During the late afternoon, the CO₂ concentration increases again as vertical mixing, decays, and as the evening traffic peak starts (around 15 h).

This analysis confirms that the coupling of the urban CO₂ emissions together with the dynamics of the ABL height is very likely a major controlling factor of the specific CO₂ diurnal pattern observed at EIF. We lack data at night and in the early morning to make a deeper analysis of the ABL dynamics and especially of the role of turbulence on CO₂ variability. We conclude that a vertical and fluctuating gradient of CO₂ likely exists above the Paris megacity, between the ground level and 317 m AGL (and likely higher). Quantifying such vertical gradients is of interest since they have to be correctly reproduced in urban mesoscale modeling frameworks for accurate atmospheric CO₂ inversion purposes. This vertical gradient can be roughly estimated by subtracting the EIF signal from the GON or the GIF signal. In the early morning (4-5 h) the GON-EIF (respectively GIF-EIF) gradient is +35 ppm (+18 ppm) in spring, +31 ppm (+17 ppm) in summer, +30 ppm (+10 ppm) in autumn, and +14 ppm (+4ppm) in winter. In the afternoon (14-16 h), the GON-EIF (respectively GIF-EIF) gradient is lower in absolute values and changes of sign: -7 ppm (-8 ppm) in spring, -4 ppm (-3 ppm) in summer, -4 ppm (-7 ppm) in autumn and -2 ppm (-5 ppm) in winter. The gradient is thus at its maximum at night and in the warm seasons, which may also reflect the influence of the biospheric respiration at the stations close to the ground level, compared to EIF. In the future, we plan to equip the Eiffel tower with two supplementary levels of sampling to collect observations that will allow us to well characterize the CO₂ vertical profile over the Paris city and its temporal variability, and its relation with ground emissions variations and their coupling with atmospheric dynamics.

3.3 Weekday versus weekend

According to the AIRPARIF inventory, the total CO₂ emissions of IdF are lower during weekends than during weekdays, with mean differences of the order of 30-40% during daytime and 50-60% during nighttime. We infer here the impact of such variations on the atmospheric concentrations. In Fig. 7, we show the mean diurnal cycles of the CO₂ concentrations at each site for each day of the week, as well as the associated standard deviation (1- σ).

In GON, the CO₂ concentrations are systematically lower over the weekend, especially on Sundays (5-10% of decrease during daytime, 25-35% of decrease during nighttime). A similar pattern is observed for MON. The weekdays-to-weekend ratios observed for the CO₂ concentrations are lower than those computed from the emissions given by the inventories. This could be due to an overestimation of the difference from the inventory ; however, biospheric fluxes (eg Schmidt et al, 2015), wind speed and direction (see section 3.5) and CO₂ background signals (see section 3.1, and Turnbull et al, 2015) are also factors that modulate the observed CO₂ concentration at each site. Disentangling the role of each of these factors on the

differences between the observed weekdays-to-weekend CO₂ concentration ratios versus the ones calculated from the inventory would require a dedicated analysis that is outside the scope of this paper. Note that while the variability of the CO₂ means is very large in GON, it is lower during weekends than during weekdays. The CO₂ diurnal cycle does not change much in GIF between a working weekday and a weekend (except for a small decrease during nighttime over the weekend), nor at EIF and TRN, possibly because of a larger influence of the biospheric fluxes (that do not depend on weekday or weekends) at these stations compared to the contribution of anthropogenic emissions (that are different on weekdays and weekends according to AIRPARIF, see Fig. 4 in Bréon et al, 2015) and that are the strongest observed at GON (sections 3.2.1 and 3.5.2). During nighttime at GIF we observed the highest concentrations from Sundays to Wednesdays, with concentrations lower by 3-5 ppm (a 20-25% decrease) from Thursdays to Saturdays. This could be due to a specific traffic pattern within the footprint of the station, but we currently do not have access to local traffic data for each day of the week to verify this hypothesis.

3.4 CO₂ seasonal cycle

We computed the seasonal cycle of CO₂ at each site, based on the monthly means of our ~1 year datasets and including all hours of the day (Fig. 8a). The seasonal cycles of the air temperature and available LBLH data (at QUA) are also shown on the same figure.

Ignoring the specific case of EIF (section 3.2.3), throughout the year we observe that the monthly mean CO₂ concentration increases with the vicinity of the station to larger CO₂ emission sources. The maximum CO₂ enhancement compared to MHD is observed at GON which is our most anthropogenically influenced station (from 6.8 ppm in July to 27.5 ppm in December). Similarly to what is observed at the diurnal scale (section 3.2), differences of several ppm are also observed between our rural sites and MHD, while the differences between the rural/peri-urban/urban stations in IdF is of the same order of magnitude. These differences of concentration between the stations located in IdF and MHD vary with the season, the seasonal cycle being much more well defined in the Paris rural stations than in MHD due to a higher biospheric activity in the IdF region than on the western coast of Ireland. This implies that background values of CO₂ in IdF (i.e. without the impact of Paris emissions) should be defined at the regional scale near Paris (~100 km) and not at the continental scale in MHD. Furthermore, in Section 3.1 we explained that the CO₂ concentration fluctuates with the origin of the airmasses that can be much variable, and therefore, specific regional background should be selected in function of the wind direction, as also mentioned for the case of Indianapolis (Turnbull et al, 2015). In conclusion, MHD appears not to be relevant as a background site for defining the atmospheric plume of CO₂ in the Paris region at the seasonal scale as well. Regional background stations (~100 km) seem to be much better suited for urban regional studies in Paris and elsewhere in the European continent. Several methods are available to extract a background signal from a timeseries (e.g. Ruckstuhl et al, 2012 ; Ammoura et al, 2016). Quantifying precisely the Paris background signals values as well as the Paris plume and its variability requires a dedicated analysis that is outside the scope of the present paper : it will specifically addressed within

another dedicated study. At each station, the monthly mean CO₂ concentration follows a seasonal cycle that reaches its maximum in winter and its minimum in summer. This is expected due to: 1/ the seasonal cycle of the biosphere; 2/ the variability of anthropogenic emissions, mainly from the heating sector, which are directly linked to ambient temperature (see 3.2.2); and 3/ the seasonal cycle of the ABL height (section 3.2.3), which is at the lowest in wintertime (e.g. Denning et al, 1995 ; Turnbull et al, 2009). It is difficult to estimate the biases due to missing data points in the time series (section 2.2.2), however as an indicator of robustness, the data coverage for each month and each station (given in Table 3) is very good overall.

To assess the variability of the seasonal cycle, Fig. 8b shows the CO₂ monthly means at each station with error bars representing the associated 1- σ standard deviation. Note that the 1- σ dispersion is the highest at GON and the lowest at MHD. More generally, the variability increases with the level of urbanization around the station and the distance to anthropogenic CO₂ emission sources. Therefore, increases in the variability from one month to the next can be used to track down the influence of more local and thus fresh sources, as a complement to the “local” wind sector (wind speed < 3 m s⁻¹). Some specific seasonal patterns can be observed:

Winter. In winter, the lower biospheric activity makes the CO₂ concentration relatively more sensitive to anthropogenic emissions (see Bréon et al, 2015). In Paris, January is usually the coldest month (meaning the month with the highest heating emissions). However, the months of December 2010 and February 2011 were characterized by cold episodes, while January 2011 was rather mild. This resulted in higher CO₂ concentrations in December and February than in January for MON and GON. In GIF, EIF and TRN, the secondary maximum (Feb.) is shifted to March. Indeed, in February, southerly winds prevailed (see S1 and also Fig. 4a and Fig. 4b), bringing Parisian anthropogenic CO₂ emissions in the direction of GON and MON and depleting the southern stations while in March, winds blew mostly from the NE/SE sectors bringing higher CO₂ levels to GIF, TRN, EIF and also MHD. The higher CO₂ concentration encountered in December compared to February or March can be explained by the ABL height being minimal in December (Fig. 8a). However, in February the GON signal remains the highest of all stations, and the concentrations observed at MON are higher than those recorded at TRN. Here we may see the impact of air masses advected from the NE with higher CO₂ background levels, and a sensitivity to upwind emissions at GON especially. Such influence of meteorological conditions on the seasonal cycle of continental stations was also reported in the literature (e.g. Fang et al., 2014; Zhang et al., 2008) and will be further assessed in section 3.5.2.

Spring. Starting in April, we observe a decrease of CO₂ at all stations except GON, as regional photosynthesis activity develops (Bréon et al., 2015). In April, the high variability of the GON signal and the prevailing local, SW and NW wind sectors show that the station experiences strong influence from anthropogenic emissions, local or advected, and explains why the CO₂ concentration remains higher than at the other stations. From April to July, we observe that the CO₂ concentration at TRN180 is always equal to or below MHD, showing the strong influence of regional biospheric activity on concentrations measured at continental stations. Indeed, this effect is also observed in TRN50 and MON in May when the biosphere is very active and winds blew mostly from the SE and SW, bringing air masses from the forests of the Centre region to IdF. During

other spring and summer months, concentrations at TRN50 and MON remain higher than at MHD as the dominant winds were from the NE sector, likely bringing emissions from the Ruhr/Benelux to MON and TRN and/or from Paris to TRN.

Summer. For all stations except GON, the annual minimum of concentration is observed in August when the following occurs : 1/ the minimum of anthropogenic emissions as given by the AIRPARIF inventory (see Fig.3 in Bréon et al, 2015);
5 2/ the maximum of photosynthetic activity (see Fig. 4 in Bréon et al); and 3/ the maximum development of the ABLH (Fig. 8a). In GON, the contribution of the local wind sector is strong in August, as confirmed by the large 1- σ deviation, explaining why the minimum of concentration is shifted to July, another month with reduced economic activity and emissions (on top of a high level of photosynthesis and a relatively high ABLH). The higher concentrations in August at GON are also associated with slow winds blowing from the northwest direction, indicating an impact of relatively local
10 emissions, possibly of the two point sources mentioned in this wind sector in section 2.1.2.

Autumn. September is characterized by an increase of the monthly mean CO₂ concentrations at all stations, although the increase is higher in GON (+9 ppm) than elsewhere (+3 to +5 ppm). As there were several local and NW events during that month, we infer that this larger increase is due to urban emissions in the vicinity of GON (eg. from CDG airport) or a bit further to the NW side of GON (among which the two industrial sites mentioned in section 2.1.2).

15 The sensitivity of the stations to wind speed and direction will be analyzed in more detail in the next section, and especially the question of higher background CO₂ levels advected from the NE sector.

3.5 Wind study: from local to regional signals

3.5.1 Wind speed effect

Wind speed is a key factor in modulating the dispersion of CO₂ emissions (e.g. Idso et al., 2002; Moriwaki et al., 2006, Rice
20 et al, 2011 ; Garcia et al, 2012 ; Lac et al, 2013 ; Turnbull et al, 2015). Figure 10 shows the mean hourly CO₂ concentrations and the associated standard deviations recorded at GON over the year of study for local afternoon hours only (11-15 h) as a function of the wind speed and colored by wind direction. The CO₂ concentrations have been seasonally adjusted to avoid biases due to seasonal variability (section 3.4), by applying the following treatment to the CO₂ hourly dataset of each station : 1/ computing the annual mean of the dataset ; 2/ computing the monthly seasonal index for each month by calculating the
25 ratio between the monthly mean and the annual mean of the dataset ; 3/ interpolating the monthly seasonal indexes at an hourly scale over the full period of study ; and 4/ dividing the CO₂ hourly dataset by the hourly seasonal index. The left panel of Fig. 9 shows that the amplitude of the CO₂ concentration range and especially the maximum values decrease exponentially with wind speed because of the ventilation and dilution effects. Such behavior is observed at all the regional stations, although the wind speed maximum is higher at TRN (~11 m s⁻¹) and even higher at EIF (~20 m s⁻¹) due to the
30 elevation of these stations. The 1- σ dispersion from the hourly means (called variability on the right panel of Fig. 9) shows a similar dependency on wind speed. At low wind speed, the relatively high level of variability can be associated to the impact of fresh and regional anthropogenic CO₂ emissions. For high wind speeds, the hourly averaged CO₂ concentration converges

towards a mean value and the $1-\sigma$ variability drops below 1 ppm. Such behavior was previously reported at former CO₂ urban stations for other cities (e.g. Garcia et al., 2012; Rice et al., 2011; Massen and Beck, 2011). However, and contrary to those studies, we do not think that this mean value can be considered as an asymptote, as it originates only from a few sparse events (spread over 7 days of the period of study), nor that it can be considered as a background CO₂ concentration for the stations.

Fig. 10 shows this CO₂ mean value at the different stations: a CO₂ horizontal enhancement appears as stations get closer to Paris city (apart from EIF), with the maximum of difference (6.6 ppm) observed between GON and MHD. The high wind speed events that occurred during the period of study correspond only to winds blowing from the southwest, mostly from the 200-220° sector. GON was thus immediately downwind of Paris emissions, most likely the reason why it exhibits the highest mean constant value. An enhancement is also observed at TRN and at GIF compared to MHD. As both TRN and GIF are located upwind of Paris, we see once again here that MHD does not provide an adequate CO₂ concentration background level for Paris and other continental Western European cities. The peri-urban upwind station of GIF has quite a similar mean constant value as the rural downwind station of MON. Indeed, MON station was not in the path of Paris CO₂ urban plume in this 20° wind sector. The EIF value is also lower than at GIF and GON, supporting the fact that for such high winds, the top of the Eiffel tower was not very sensitive to surface emissions, most likely because between 0 and 300m AGL, ventilation of emissions was stronger than their vertical mixing.

3.5.2 Fine wind sector analysis

In order to distinguish the relative contributions of the local, the remote and the Paris megacity regional CO₂ fluxes to the CO₂ concentration observed at the 5 stations of the Paris network, we analyzed the dependence of the observed CO₂ concentration and its variability on the horizontal wind speed and direction. Considering the diurnal variability of vertical transport dynamics (section 3.2), we separately analyzed afternoon (11 h to 15 h) and nighttime (22 h to 2 h) data. For the TRN station, we consider that the TRN50 level is sufficient for this analysis.

Inner Paris extends to a diameter of 10 km, while the Paris metropolitan area extends to a diameter of 30 to 50 km. The distance of the peri-urban stations GON and GIF to the Paris inner city is about 10 km and 15 km, respectively. The distance of the rural stations MON and TRN to inner Paris is about 30 and 100 km, respectively. Taking into account these distances, we set the hypothesis that we can assess the influence of local emissions using hourly means observed in low wind speed conditions (less than 3 m s^{-1}) while the influence of remote emissions can be analyzed using data recorded in relatively high wind speed conditions (more than 8 m s^{-1}). This relies on considering the time given for atmospheric mixing of local and regional emissions (dominant at low to mid windspeeds) versus their ventilation (dominant at high windspeeds) : the integration of local and regional emissions into an air mass, which carries the signature of remote emissions when it is upwind of Paris, gets higher with decreasing windspeeds. For example, for windspeeds lower than 3 m.s^{-1} (11 km.h^{-1}), it takes one hour or more for any airmass to flow over the center of Paris (~10 km of diameter), allowing some time for local

emissions to get mixed into the airmass, while at $8 \text{ m}\cdot\text{s}^{-1}$ or more ($\sim 29 \text{ km}\cdot\text{h}^{-1}$) it takes about 20 minutes or less, allowing less time for the atmospheric integration of local to regional emissions. In the middle range of windspeed ($3\text{-}8 \text{ m}\cdot\text{s}^{-1}$), we expect most of the CO_2 variability to be driven by the influence of the regional emissions coming from Paris.

For all of the regional stations, Fig. 11 shows the pollution roses of the mean afternoon CO_2 concentration binned by wind speed (ws) and wind direction (wd) with a resolution of $1 \text{ m}\cdot\text{s}^{-1}$ for ws and 10° for wd. We use here the CO_2 hourly concentration dataset that has been seasonally adjusted (section 3.5.1). In order to assess the representativeness of each (ws, wd) bin, the contribution of each concentration mean for a given (ws, wd) bin on the total concentration is also calculated, after applying a square root transformation on the CO_2 concentration to reduce any bias from the highest CO_2 values (we used the polarFreq function from the OpenAir workpackage for R with the option “weighted mean” – more information can be found online here : http://www.openair-project.org/PDF/OpenAir_Manual.pdf). We also show the mean $1\text{-}\sigma$ standard deviation of the CO_2 concentration at each bin. A similar figure for nighttime data is given in the supplementary material S6a. During daytime (nighttime), the color scale is limited to the 380-430 ppm interval for the CO_2 concentration and to the 0-5 ppm range for the standard deviation. There are a few values outside of these ranges that are forced to the closest range bound value. To facilitate the comparison between the stations, the highest complete wind speed circle visible on the plots is set at $10 \text{ m}\cdot\text{s}^{-1}$ in all cases. For MON, GON and GIF, all the data are plotted when taking this wind speed threshold. For TRN and EIF, wind speeds can reach higher values due to the elevation of these stations (during the afternoon: up to $15 \text{ m}\cdot\text{s}^{-1}$ at TRN and $25.5 \text{ m}\cdot\text{s}^{-1}$ at EIF; at night: up to $15 \text{ m}\cdot\text{s}^{-1}$ at TRN and $22 \text{ m}\cdot\text{s}^{-1}$ at EIF). Although they represent only a minor fraction of the datasets, some of the TRN and EIF data are thus not apparent on Fig. 11: the plots for the full wind speed ranges encountered at EIF and TRN are given in the Supplementary material S6b (daytime) and S6c (nighttime).

20

Influence of remote emissions (> 100 km)

The back trajectories (S1) show that Paris was exposed to a range of synoptic air masses over the period of study, including clean oceanic ones and others with CO_2 enriched by remote anthropogenic emissions especially from the Benelux, the Ruhr area and the London megacity. Relatively high CO_2 concentrations ($> 410 \text{ ppm}$) were observed for high wind speeds ($> 8 \text{ m}\cdot\text{s}^{-1}$) in the $0\text{-}45^\circ$ NNE sector at the 3 stations located relatively close to the ground level (MON, GON and GIF). For the elevated stations (EIF and TRN), such concentration values also occur, but as expected at higher wind speeds ($> 12\text{-}14 \text{ m}\cdot\text{s}^{-1}$), reaching at least the 410 to 420 ppm range at all of the stations. The fraction of data falling in these (ws, wd) bins is large enough to consider these high concentration values to be statistically representative. Furthermore, the standard deviation of the signal at the upwind stations is quite low (less than 0.6 ppm), which indicates that the high concentration values observed upwind of Paris (GON and MON) are not associated with fresh emissions, but with imported pollution that was already well-mixed in the atmosphere. It is likely that we see here the signature of remote anthropogenic CO_2 emissions from hot spots such as the Benelux and the Ruhr areas that bring higher CO_2 background levels to all the stations. The high CO_2 concentrations observed in the $0\text{-}35^\circ$ NE sector at the downwind stations (EIF, GIF and TRN50) for moderate to high wind conditions ($\geq 3 \text{ m}\cdot\text{s}^{-1}$) appear thus to be due not only to the Paris CO_2 emissions plume, but also to enriched background CO_2

levels advected from the NE. By comparison, the background levels that are observed in the 200° (SE) to 280° (NW) sector of GIF and TRN50 are lower than 400 ppm, while the 0-35° NE background levels at GON and MON are often above 400 ppm, reaching concentrations in the 410-430 ppm range. This shows that the Paris megacity background values can vary by several ppm depending on the wind direction, with the highest CO₂ concentrations advected in the 0-45° wind cone. We note also that EIF shows higher concentrations in the 295-360° NW sector at high wind speeds that could be associated with long-range transport of anthropogenic plumes from the northern emissions hot spots emissions mentioned and better seen at this elevated station. Also, TRN shows higher CO₂ concentrations in the 345-360° NW sector for high wind speeds, that could be attributed to these hot spots - but also to Paris.

During nighttime, for wind speeds higher than 8 m s⁻¹ all stations show higher CO₂ levels in the 0-45° NE sector than in the other wind directions (see Fig.S6a).

Influence of local emissions (< 10 km)

In section 3.2.1, we questioned whether MON was under the strong influence of local signals. The MON CO₂ wind rose shows that for wind speeds in the 0-2 m s⁻¹ range, higher CO₂ concentration (400 ppm to more than 430 ppm) are observed in different wind sectors. Note the 230°-240° SW sector, where the bin contribution is the highest (~0.8-1%). These higher CO₂ concentrations can most likely be attributed to the influence of the point sources relatively close to MON mentioned in section 2.1.2, but also to relatively close diffuse emissions (traffic, heating...) from ground activity under the path of the air mass, but also possibly to aircraft emissions. Montgé-en-Goële is located in the path of aircraft departing from CDG for easterly winds and of aircraft arriving to that airport for westerly winds (<http://www.advocnar.fr/Fluxdetrajectoires.html>). The CDG platform is equipped with two runways (North and South) from which the planes both take off and land along two W-E axis and pass very close the station at altitudes between 0 and 1000 m AGL. The NW and SE sides of the station are exposed to aircraft flying respectively to and from the CDG northern runway, while the 260°-360° sector and the 180°-260° sectors are the most exposed to aircraft traffic from the southern runway. Tarmac and in flight aircraft traffic (below 915 m ASL) are estimated to represent ~60% of the airport emissions (ADP, 2013). Apart from road traffic emissions to and from CDG, the airport infrastructure itself (building heating, stopover airplanes electricity supply...) could also influence the station (as it represents ~11% of the airport CO₂ emissions; ADP, 2013), although more likely at the regional scale (see below). A much weaker influence of the Le Bourget aircraft flight paths, passing a few km southern than CDG airplanes but also at low altitude, is also possible at the southern side of the station.

In sections 3.2.1 and 3.4, we questioned the influence of local sources on GON (such as CDG and Le Bourget airports, but also of point sources mentioned in section 2.1.2 and diffuse sources around the station). As for MON, all these types of sources in the vicinity of GON will likely influence it at low windspeed. GON is also exposed to aircraft emissions as it lies close to the lowest flight paths (0-1000m AGL) from the CDG and Le Bourget airports (<http://www.advocnar.fr/Fluxdetrajectoires.html>). These emissions are due: (i) in the NW sector, to takeoffs from the CDG northern runway; (ii) in the SW sector, to takeoffs from the CDG southern runway and from Le Bourget runway; (iii) in the

NE sector, to landing on both CDG runways; and (iv) in the SE sector, to landings on the southern runway of CDG and to a lesser extent on Le Bourget airport. Also, it is likely that GON gets exposed to emissions from the two airports themselves, located a few km away. Note that the standard deviation which is more than 1 ppm higher from 60° (NE) to 170° (SE) seems to indicate fresher emissions in this wind sector. Nearby highways (located about 1.2 km north and east) could contribute in
5 these wind directions. Discriminating between the different emission sources influencing the GON or the MON stations at low windspeed would require dedicated fine scale modeling studies that are outside the scope of this study.

At EIF, the influence of local emissions is expected mostly between the late morning and the late afternoon since, as we have seen in section 3.2.2, the top of the Eiffel tower receives surface emissions in this time period during all seasons. The CO₂ pollution rose of Fig. 11 indicates high concentrations (400 ppm to more than 430 ppm) in all directions around the stations
10 for wind speeds comprised between 0 and 2 m s⁻¹. The variability is quite large (1.5 to 5 ppm) indicating fresh emissions and reflecting the spatial and temporal variability of the emissions coupled to atmospheric transport variations. Carbon isotopes and CO₂ co-emitted species measurements would be useful here to estimate the role of the different emission sectors (ex. Lopez et al, 2013).

In GIF, a few high CO₂ spikes are observed for low wind conditions in diverse wind directions. These spikes are likely due
15 to emissions from traffic and heating from the surrounding infrastructures, as observed from the corresponding relatively high standard deviation (> 5 ppm). Flight paths to and from Orly airport for westerly winds pass several km south of the station and likely have a weak local impact.

Similarly to what is observed at GIF, higher CO₂ concentrations are observed at TRN50 in the wind sector of the city of Orleans, located ~13 km SW of the station.

20 At night, MON and GIF show a higher local influence that still remains moderate. At EIF, no specific local influence is observed apart from a couple of (ws, wd) bins, confirming that the station is quite disconnected from the surface where urban emissions are diluted into the nocturnal layer. At GON, the influence of local emissions is strongly evident, with CO₂ concentrations reaching greater than 460 ppm and standard deviation greater than 5 ppm. In the 2-3 m s⁻¹ range, the station shows the highest CO₂ concentration in the direction of the CDG airport, a source that seems to have an impact on GON
25 even at night. CDG is one of the only airports in Europe to have nocturnal activity. TRN seems to be less influenced by local emissions than during daytime. TRN not being impacted by Paris urban heat island, the nocturnal boundary layer is very shallow there so that the 50 m level is probably often decoupled from fresh emissions during the night (Pal et al, 2012).

At all stations, except for a few points in the SW sector at MON and GIF, the bin contribution of the data recorded for wind speeds in the 0-3 m s⁻¹ range is quite low, which indicates that generally the low wind conditions do not bias the data very
30 much. However, since local sources can be relatively strong, for regional studies these local influences should be removed by filtering out the CO₂ concentrations collected at wind speeds lower than 3 m s⁻¹.

Influence of regional emissions (10-100 km)

Most of the data correspond to wind speeds between 3 and 8 m s⁻¹, values for which we expect the regional influence of the Paris megacity on the downwind observed CO₂ concentrations to be the highest.

In the 0°-45° (NNE) sector, we observe relatively high CO₂ signals (>400 ppm) and low standard deviation values, even in stations upwind of Paris (GON and MON). In MON, the CO₂ concentrations in this wind sector are even higher than the ones in the SW sector which is expected to be exposed to the Paris emissions plume. This large NE signal can be attributed to the impact of remote emissions advected from that wind sector, as observed for higher wind speeds. In EIF and GIF (over and downwind of Paris in that wind sector), the CO₂ concentration reaches even higher values (>430 ppm, especially in EIF), which indicates the additional impact of the urban regional emissions. The contribution of each (ws, wd) bin is in the 0.4-1% range and is thus significant. These high concentrations are associated with high standard deviations (> 1 ppm, and even > 5 ppm at EIF), which results both from the high spatial and temporal variability of fresh emissions at the surface and from small scale dynamic effects in the ABL such as turbulence (succession of updrafts bringing polluted air to the station and downdrafts bringing cleaner air). In TRN50, there are some bins where the signal is higher than in MON and GON, but overall, the CO₂ concentration is lower, indicating that the Paris plume does not pass the TRN tower (50 m level) very often. In the 45-90° (ENE) sector, all stations but EIF show CO₂ concentrations mostly in the 390-400 ppm range with some bins in the 400-410 ppm range. EIF shows more bins in the 400-410 ppm range, showing a higher exposure to urban emissions. However, while the standard deviation is relatively low in MON and TRN50, this is not the case at the GON, EIF and GIF stations, likely due to a higher proximity to sources of emissions, that, for GON include the CDG airport.

In the SW wind direction, stations upwind of the Parisian emissions (TRN50 and GIF) mostly show CO₂ concentrations in the 380-400 ppm range. In EIF, and even more in GON, we observe higher CO₂ values reaching the 400-410 ppm range. Due to its geographical position, EIF is less exposed to Parisian emissions in this wind sector, while GON is directly downwind of Paris for the 175-235° wind sector, where the largest point contribution reaches 1.6%. The standard deviation in EIF is above 1 ppm although lower than in the NE sector, while it is less than 1 ppm in GON, indicating that the emissions were mixed before arriving at the station. The MON station does not show specifically higher CO₂ concentrations compared to the upwind GIF station, except in the direction of the CDG airport. This latter source together with industrial emissions as well as other sources (highways, domestic and commercial heating...) located in this direction (Fig.1) seems to have more impact on the station than the Paris emissions plume, which does not appear to often advect to the station.

In the NW wind sector, all stations except EIF are mostly in the 390-400 ppm range, with some values in the 400-410 ppm range (like in the 45-90° sector or NNE sector). EIF exhibits higher concentrations in the 325-360° sector, with values often in the 410-430 ppm range, and even reaching more than 430 ppm. The associated standard deviation is also very high at EIF, in the 2-5 ppm range and even more, indicating that emissions from the NW of Paris strongly impact this station. On the contrary, the variability is mostly below 1 ppm in the other stations. The highest values are observed at GIF in the 305-325° direction, which could be explained by the station receiving emissions from the Saint-Quentin-en-Yvelines metropolitan area located 10-15 km upwind of GIF in those wind directions.

In the SE wind sector, for moderate wind speeds the MON, GIF and TRN50 stations show CO₂ concentrations mostly below 400 ppm and a few (ws, wd) bins in the 400-410 ppm range, especially in GIF for the 3-4 m s⁻¹ range and in the 90-135° sector. This sector comprises the southern branch of the extension of the Paris megacity which likely impacts the station. It is surprising though, that the 70-85° (ENE) sector does not show similar concentration ranges as it is urbanized at a similar level. At GON, the station is mostly sensitive to emissions in the 135-180° (SSE) sector although the standard deviation is quite low indicating these emissions are not from nearby sources as they are already mixed into the atmosphere. The EIF signal is as high as in the NW sector, very variable from one wind direction to the next and shows a high standard deviation, again reflecting the large variability of surface emissions and possibly the impact of atmospheric turbulence on the observations.

At night, MON exhibits the highest CO₂ concentrations in the 0-45° (NNE) sector with values reaching the 410-420 ppm range. Those higher concentrations probably correspond to the continental background signals of polluted air masses advected from the Benelux and Ruhr areas. At GON, the CO₂ concentration reaches similar values but in all directions, showing on top of higher NE background values an impact of the regional urban emissions. As during daytime, EIF shows higher concentrations in the urbanized sectors upwind of the station (NE, SE and NW mainly), although the concentrations stay mostly below 410 ppm - as a result of the decoupling from surface emissions during nighttime. At GIF, the highest concentrations are encountered, like during daytime, mostly in the NE sector that is the most exposed to Paris emissions. At TRN some (ws, wd) bins show higher CO₂ concentration in the NE sector, although this remains at a moderate level. The levels of the standard deviation confirm these observations and the data distribution plots show that generally most of the regional signal is contained into the 3-6 m s⁻¹ range.

20

4 Conclusions

This work forms the first study of ~1-year of measurements of atmospheric CO₂ in the region of the Paris megacity. We analyzed the CO₂ diurnal, synoptic and seasonal variability at five stations in that region and carried out a comparison with the CO₂ dataset recorded at the MHD remote site.

In all stations of the Paris network, the influence of anthropogenic emissions, biospheric fluxes, atmospheric dynamics and synoptic wind patterns were shown to be key factors of the diurnal, weekday/weekend and seasonal variability of the atmospheric CO₂ concentrations.

At low wind speed, the stations receive local emissions from sources that could extend to a few kilometers, leading to a build-up of the CO₂ concentration, especially over Paris at the top of the Eiffel tower during daytime and at the GON peri-urban station, where the concentration increase can reach up to 60 ppm. For wind speed values comprised between 3 and 9 m s⁻¹, advection leads to a decrease of the CO₂ concentration at all stations by ventilation of the emissions. For wind speeds higher than 9 m s⁻¹, as it was mentioned in previous urban studies, the CO₂ concentration tends toward a mean constant

value. However, contrary to previous studies, we showed that this value is different at each site and increases with the level of urbanization surrounding the station, leading to an enhancement of a few ppm at downwind stations compared to upwind ones. We argued that this value is based only on sparse meteorological events so that it cannot be defined as an asymptotic value, nor should it be used as a regional background.

5 Our work shows large diurnal and seasonal differences in the CO₂ concentration between the MHD site and the Paris upwind sites, as advected air masses undergo the influence of sources and sinks of CO₂ encountered on their footprint before reaching the megacity. We demonstrated that such a remote coastal site should not be used as a background site to infer atmospheric regional CO₂ signals (~100 km) coming from emissions of urbanized regions located several hundreds of kilometers away from this remote site on the continent, as it was done in some previous studies. A similar conclusion was also highlighted by Turnbull et al (2015) when analyzing atmospheric CO₂ variability in the Indianapolis region. Furthermore, even at high wind speeds, higher CO₂ concentrations (up to several ppm) are observed for air masses advected from the 0-45° NNE sector at all of the regional stations, compared to those advected from the SW sector, highlighting the impact of anthropogenic emissions from remote hot spots like Benelux and the Ruhr valley on the Paris region CO₂ background in the NNE sector. Indeed, the average CO₂ concentrations measured at a given station when it is located downwind the Paris megacity are not always higher than the concentrations measured at that same station when it is located upwind, and this concerns both the hourly, diurnal and seasonal averages. This shows that the CO₂ concentration advected from the polluted 0-45° NNE sector can overtake the sum of the CO₂ plume out coming from Paris for SW winds and of the relatively low SW oceanic CO₂ background signals. This leads to the conclusion that when further developing the Paris CO₂ network, efforts must be made to carefully set-up several regional background sites on the path of the different wind directions and ideally at the peri-urban/rural border of the city to constrain its signal as much as possible. Ideally, the network will also be designed to position the urban and peri-urban downwind sites on these same wind directions axes. The CO₂ datasets presented here provide the basis for a study conducted on atmospheric inversion modeling of the Paris CO₂ emissions (Staufner et al, 2016), where we quantified the need of 8 more sites in the suburban/urban border of Paris to improve our top-down approach.

25 Furthermore, our analysis shows the strong coupling that exists between the CO₂ concentration diurnal cycle and the boundary layer height cycle at the elevated stations and especially at EIF. We also highlighted how the high variability observed at EIF in the afternoon reflects the coupling of the highly variable urban emissions in the vicinity of the station with fluctuations of the wind speed and direction but also possibly with atmospheric fine scale dynamic processes. These results have consequence on the assimilation of the EIF data for inverse modelling purposes. Tall towers have been for several years the first choice in matter of sites selection for studying atmospheric CO₂ at the regional to the continental scales (e.g. Andrews et al., 2014; Haszpra et al., 2015; Gloor et al., 2001; Vermeulen et al., 2011), but their use for understanding CO₂ in urban environment seems to be more complicated as this requires the proper representation of the underlying dynamic processes (including turbulence) that occur inside the boundary layer, and their coupling with the highly variable ground anthropogenic CO₂ emissions. For these reasons, we are for now not able to use data from EIF in our inverse

modelling framework (Bréon et al., 2015). We plan to improve our instrumental set-up on the Eiffel tower with two additional sampling heights to gather vertical CO₂ profiles and associated meteorological data : this will be of great help to understand the coupling between CO₂ sources and atmospheric dynamics over the Paris megacity in the future. This recalls as well that the altitude relative to ground level and the distance to the emissions of a station are very important factors to take into account in the network capacity to properly detect a CO₂ urban plume (see also the discussion about this topic in Boon et al., 2015).

About gaining lessons on urban CO₂ network design, with 13 observation towers located in and just around the city, the Indianapolis network is a good example to follow (see Turnbull et al, 2015) - as long as the budget allow it - that fulfills the urban network constrains we inferred from our analysis in Paris. Longer prospects on the Paris network design with cheaper sensors are discussed in the study of Wu et al (2016). Note that these lessons are appropriate to cities having a flat continental topography. The situation would be different for coastal or mountain/valley cities, where complex meteorological features occur (breezes, katabatic winds, thermal inversion...).

The fine classification of the CO₂ concentrations collected at each site following wind directions and wind speeds allowed us to better define the footprint of each station and the impact of local, regional and remote CO₂ fluxes on each station. In each of the regional sites, the high CO₂ concentrations observed at low wind speeds (<3 m s⁻¹) revealed the impact of local sources including likely emissions from aircraft and airports, cement plants and thermal plants. For moderate wind speeds (3 to 9 m s⁻¹), the impact of the CO₂ emissions of Paris is clearly seen at urban and peri-urban stations (GON, EIF and GIF) in the afternoon, and much less at night. This impact however is barely seen in the two rural stations (MON and TRN), and ultimately do not seem to be relevant sites to study the CO₂ emission plume from the Paris megacity.

At each station, the minimum of the seasonal cycle amplitude was found in summer due to high photosynthesis, lower anthropogenic emissions and higher ABL height. The maximum of the CO₂ seasonal cycle was found in winter when the biospheric activity reaches its minimum, the Paris anthropogenic emissions get to their maximum and the ABL height is at its lowest. However, we could not separate the anthropogenic and biospheric CO₂ signals, nor the role of the different emission sectors. This highlights the need for regular carbon isotopic measurements of CO₂ at the regional network stations, together with measurements of anthropogenic co-emitted species such as CO, NO_x, black carbon and volatile organic compounds (e.g. Lopez et al., 2013; Ammoura et al., 2014; Ammoura et al., 2015). Finally, we show that ancillary data such as local meteorological data and parameters defining the structure of the atmosphere such as the ABL height are very important to understand the observed CO₂ variability. Ideally, such measurements should also be included in the development of future urban CO₂ monitoring networks.

30

5 Data availability

The CO₂-Megaparis datasets are available from the AERIS/ESPRI data center via the following secure FTP link: <http://cds-espri.ipsl.fr/espri/pubipsl/co2-megaparis/ftp.html> upon simple request to the first author. The ICOS datasets are available from the ICOS database at LSCE. Please contact the first author for further information (irene.remy-xueref@univ-amu.fr).

Supplement link

5 Acknowledgments

This work was mostly funded by the Agence Nationale de la Recherche (ANR) in the framework of the CO₂-Megaparis project and partly by the Ville de Paris through the “Le CO₂ parisien” (Paris 2030) project. We deeply acknowledge AIRPARIF technical team for the maintenance of the CO₂-Megaparis stations. The authors are very grateful to the RAMCES-ICOS team and they also thank Sandip Pal for technical help. The GIF and TRN stations are funded by INSU and
10 CEA (SNO RAMCES/ICOS). Most of the figures shown in this work were produced with the Openair package for R (Carslaw and Ropkins, 2012; Carslaw, 2015). We especially acknowledge David Carslaw (Openair package) for helpful advices. We thank very much SPR at CEA Saclay for providing us with the meteorological measurements. The first author sends warm acknowledgments to Peter Rayner and Thomas Lauvaux for their scientific advices in building-up the CO₂-Megaparis project, and to Cecilia Garrec and Peter Rayner (once again) for their help in coordinating it. Special thanks to
15 Steve Wofsy for his support and to Chris Rella from the Picarro company for his help with the CRDS analyzers.

References

- ADP: Aéroports de Paris, <http://www.aeroportsdeparis.fr/groupe/rse/engagements/maitrise-des-impacts/air-emissions-et-climat/bilan-emissions-aeroportuaires>, 2013.
- AIRPARIF: Bilan des émissions de polluants atmosphériques et de gaz à effet de serre en Ile-de-France 2005, 2010
20 (http://www.airparif.asso.fr/_pdf/publications/Rinventaire_2005_201004.pdf).
- AIRPARIF: Bilan des émissions de polluants atmosphériques et de gaz à effet de serre en Île-de-France pour l’année 2010 et historique 2000/2005, 2013 http://www.airparif.asso.fr/_pdf/publications/inventaire-emissions-idf-2010-rapport-130731.pdf.
- Ammoura, L., Xueref-Remy, I., Gros, V., Baudic, A., Bonsang, B., Petit, J. E., Perrussel, O., Bonnaire, N., Sciare, J., and Chevallier, F.: Atmospheric measurements of ratios between CO₂ and co-emitted species from traffic: a tunnel study in the
25 Paris megacity, *Atmos. Chem. Phys.*, 14, 12871-12882, doi:10.5194/acp-14-12871-2014, 2014.
- Ammoura, L., Xueref-Remy, I., Vogel, F., Gros, V., Baudic, A., Bonsang, B., Delmotte, M., Té, Y., and Chevallier, F.: Exploiting stagnant conditions to derive robust emission ratio estimates for CO₂, CO and volatile organic compounds in Paris, *Atmos. Chem. Phys.*, 16, 15653-15664, doi:10.5194/acp-16-15653-2016, 2016.

- Andrews, A. E., Kofler, J. D., Trudeau, M. E., Williams, J. C., Neff, D. H., Masarie, K. A., Chao, D. Y., Kitzi, D. R., Novelli, P. C., Zhao, C., Dlugokencky, E., Lang, P. M., Crotwell, M. J., Fischer, M. L., Parker, M. J., Lee, J. T., Baumann, D. D., Desai, A. R., Stanier, C. O., De Wekker, S. F. J., Wolfe, D. E., Munger, J. W., and Tans, P. P.: CO₂, CO, and CH₄ measurements from tall towers in the NOAA Earth System Research Laboratory's Global Greenhouse Gas Reference Network: instrumentation, uncertainty analysis, and recommendations for future high-accuracy greenhouse gas monitoring effort, *Atmos. Meas. Tech.*, 7, 647–687, 2014, doi: 10.5194/amt-7-647-2014.
- Apadula, F., Gotti, A., Pigini, A., Longhetto, A., Rocchetti, F., Cassardo, C., Ferrarese, S., and Forza, R.: Localization of source and sinks regions of carbon dioxide through the method of the synoptic air trajectory statistics, *Atmos. Environ.*, 37, 3757–3770, doi: 10.1016/S1352-2310(03)00505-3, 2003.
- Artuso, F., Chamard P., Piacentino S., Sferlazzo D., De Silvestri L., di Sarra A., Meloni D., and Monteleone F.: Influence of transport and trends in atmospheric CO₂ at Lampedusa, *Atmosph. Environ.*, 43, 19, 3044, doi: 10.1016/j.atmosenv.2009.03.027, 2009.
- Biraud, S., Ciais, P., Ramonet, M., Simmonds, P., Kazan, V., Monfray, P., O'Doherty, S., Spain, T. G., and Jennings, S. G.: European greenhouse gas emissions estimated from continuous atmospheric measurements and radon 222 at Mace Head, Ireland, *J. Geophys. Res.*, 105(D1), 1351–1366, doi: 10.1029/1999JD900821, 2000.
- Boon, A., Broquet, G., Clifford, D. J., Chevallier, F., Butterfield, D.M., Pison, I., Ramonet, M., J.D. Paris, J. D., and Ciais, P.: Analysis of the potential of near ground measurements of CO₂ and CH₄ in London, UK for the monitoring of city-scale emissions using an atmospheric transport model, *Atmos. Chem. Phys. Discuss.*, 15, 33003–33048, doi: 10.5194/acpd-15-33003-2015, 2015.
- Bousquet, P., Gaudry, A., Ciais, P., Kazan, V., Monfray, P., Simmonds, P. G., Jennings, S., and O'Connor, T.: Atmospheric CO₂ concentration variations recorded at Mace Head, Ireland, from 1992 to 1994, *Phys. Chem. Earth*, 21, 477–481, 1996.
- Bréon, F. M., Broquet, G., Puygrenier, V., Chevallier, F., Xueref-Remy, I., Ramonet, M., Dieudonné, E., Lopez, M., Schmid^h M., Perrussel, O., and Ciais, P.: An attempt at estimating Paris area CO₂ emissions from atmospheric concentration measurements, *Atmos. Chem. Phys.*, 15, 1707-1724, doi: 10.5194/acp-15-1707-2015, 2015.
- Cantat, O.: « L'îlot de chaleur urbain parisien selon les types de temps », *Norois*, 191, 75-102, 2004.
- Carslaw, D.C. and K. Ropkins, *Openair* — an R package for air quality data analysis. *Environmental Modelling & Software*. Volume 27-28, pp. 52–61, 2012.
- Carslaw, D.C., *The openair manual* — open-source tools for analysing air pollution data. Manual for version 1.1-4, King's College London, 2015.
- Denning, A.S., Fung, I.Y., and Randall, D., Latitudinal gradient of atmospheric CO₂ due to seasonal exchange with land biota, *Nature*, 376, 240-243, 1995.
- Denning, A.S., Rayner, P.J., Law, R.M., and Gurney, K.R. : Atmospheric tracer transport model intercomparison project (TransCom), IGBP/GAIM report series, Report #4, Ed. D. Sahagian, 1995.

- Dieudonné, E., Multi-instrumental analysis of the influence of boundary layer depth variability on the vertical distribution of nitrogen oxides in Paris region, Ph.D. thesis, Université Pierre et Marie Curie, Paris, France, 2012, in French (<http://tel.archives-ouvertes.fr/tel-00807665>).
- Dieudonné, E., Ravetta, F., Pelon, J., Goutail, F., and Pommereau, J. P., Linking NO₂ surface concentration and integrated content in the urban developed atmospheric boundary layer, *Geophys. Res. Lett.*, 40, 1247-1251, doi: 10.1002/grl.50242, 2013.
- Duren, R. M. and Miller, C. E.: Measuring the carbon emissions of megacities, *Nature Climate Change*, 2, 560-562, doi:10.1038/nclimate1629, 2012.
- Fang, S. X., Zhou, L. X., Tans, P. P., Ciais, P., Steinbacher, M., Xu, L., and Luan, T.: In situ measurements of atmospheric CO₂ at the four WMO/GAW stations in China, *Atmos. Chem. Phys.*, 14, 2541-2554, doi:10.5194/acp-14-2541-2014, 2014.
- Garcia, M. A., Sanchez, M. L., and Perez, I.: Differences between carbon dioxide levels over suburban and rural sites in Northern Spain, *Environ. Sci. Pollut. Res.* 19: 432-439, doi:10.1007/s11356-011-0575-4, 2012.
- Garcia, M. A., Sanchez, M. L., and Perez, I. A., Synoptic weather patterns associated with carbon dioxide levels in Northern Spain, *Sci. Total Environ.*, 408, 3411-3417, doi: 10.1016/j.scitotenv.2010.04.034, 2010.
- Gerbig, C., Lin, J. C., Munger, J. W., and Wofsy, S. C.: What can tracer observations in the continental boundary layer tell us about surface-atmosphere fluxes?, *Atmos. Chem. Phys.*, 6, 539-554, doi:10.5194/acp-6-539-2006, 2006.
- George, K., Ziska, L. H., Bunce, J. A., and Quebedeaux, B.: Elevated atmospheric CO₂ concentration and temperature across an urban-rural transect, *Atmos. Environ.*, 41, 7654-7665, doi: 10.1016/j.atmosenv.2007.08.018, 2007.
- Gloor, M., Bakwin, P., Hurst, D., Lock, L., Draxler, R., and Tans, P.: What is the concentration footprint of a tall tower?, *J. Geophys. Lett. Atm.*, 106 (D16), 17831–17840, doi: 10.1029/2001JD900021, 2001.
- Gratani, L. and Varone, L.: Daily and seasonal variation of CO₂ in the city of Rome in relationship with the traffic volume, *Atmos. Environ.* 39, 2619-2624, doi: 10.1016/j.atmosenv.2005.01.013, 2005.
- Grimmond, C. S. B., King, T. S., Cropley, F. D., Nowak, D. J., and Souch, C.: Local-scale fluxes of carbon dioxide in urban environments: methodological challenges and results from Chicago, *Environ. Pollut.*, 116, S243–S254, doi: 10.1016/S0269-7491(01)00256-1, 2002.
- Gurney, K. R., Law, R. M., Denning, A. S., Rayner, P. J., Baker, D., Bousquet, P., Bruhwiler, L., Chen, Y. H., Ciais, P., Fan, S., Fung, I. ., Gloor, M., Heimann, M., Higuchi, K., John, J., Maki, T., Maksyutov, S., Masarie, K., Peylin, P., Prather, M., Pak, B. C., Randerson, J., Sarmiento, J., Taguchi, S., Takahashi, T. and Yuen, C. W.: Towards robust regional estimates of CO₂ sources and sinks using atmospheric transport models, *Nature*, 415, 626-630, doi:10.1038/415626a, 2002.
- Haszpra, L., Barcza, Z., Haszpra, T., Pátkai, Z., and Davis, K. J.: How well do tall tower measurements characterize the CO₂ mole fraction distribution in the planetary boundary layer?, *Atmos. Meas. Tech. Discuss.*, 7, C5097–C5097, doi: 10.5194/amt-8-1657-2015, 2015.

- Hazan, L., Tarniewicz, J., Ramonet, M., Laurent, O., and Abbaris, A.: Automatic processing of atmospheric CO₂ and CH₄ mole fractions at the ICOS Atmosphere Thematic Centre, *Atmos. Meas. Tech.*, 9, 4719-4736, doi:10.5194/amt-9-4719-2016, 2016.
- IAU, L'environnement en Ile-de-France Mémento, Fiche climatique n° 12, Institut d'Aménagement et d'Urbanisme Ile-de-France, Etude 953, Janvier 2013 (http://www.iau-idf.fr/fileadmin/Etudes/etude_953/12_FicheCLIMATIQUE.pdf).
- 5 Idso, C. D., Idso, S. B., and Balling, Jr., R. C.: The urban CO₂ dome of Phoenix, Arizona, *Physic. Geograp.*, 19 (2), 95-108, doi:10.1080/02723646.1998.10642642, 1998.
- Idso, C. D., Idso, S. B., and Balling, Jr., R. C.: An intensive two-week study of an urban CO₂ dome in Phoenix, Arizona, USA, *Atmos. Environ.* 35 (6), 995–1000, doi:10.1016/S1352-2310(00)00412-X, 2001.
- 10 Idso, S. B., Idso, C. D., and Balling, Jr., R. C.: Seasonal and diurnal variations of near-surface atmospheric CO₂ concentration within a residential sector of the urban CO₂ dome of Phoenix, AZ, USA, *Atmos. Environ.*, 36 (10), 1655–1660, [http://dx.doi.org/10.1016/S1352-2310\(02\)00159-0](http://dx.doi.org/10.1016/S1352-2310(02)00159-0), 2002.
- IEA, World Energy Outlook Ch.8, 179-193, International Energy Agency, 2008.
- INSEE, La population légale de l'Ile-de-France au 1^{er} janvier 2010, n° 298, 2012.
- 15 Kennedy, C., Ramaswani, A., Carey S., and Dhakal S.: Greenhouse Gas Emission Baselines for Global Cities and Metropolitan Regions, Paper prepared on requests from the World Bank and presented at the plenary of 5th Urban Research Symposium on Cities and Climate Change, Marseille (France), 28-30 June 2009.
- Lac, C., Donnelly, R. P., Masson, V., Pal, S., Riette, S., Donier, S., Queguiner, S., Tanguy, G., Ammoura, L., and Xueref-Remy, I.: CO₂ dispersion modelling over Paris region within the CO₂-MEGAPARIS project, *Atmos. Chem. Phys.*, 13, 4941-4961, doi:10.5194/acp-13-4941-2013, 2013.
- 20 Lauvaux, T., Miles, N., Deng, A., Richardson, S.J., Cambaliza, M.O., Davis, K.J., Gaudet, B., Gurney, K.R., Huang, J., O'Keefe, D., Song, Y., Karion, A., Oda, T., Patarasuk, R., Sarmiento, D., Shepson, P., Sweeney, C., Turnbull, J., and Wu, K.: High-resolution atmospheric inversion of urban CO₂ emissions during the dormant season of the Indianapolis Flux Experiment (INFLUX), *J. Geophys. Res. Atmos.*, 121, 5213–5236, doi:10.1002/2015JD024473, 2016.
- 25 Lauvaux, T., Schuh, A. E., Uliasz, M., Richardson, S., Miles, N., Andrews, A. E., Sweeney, C., Diaz, L. I., Martins, D., Shepson, P. B., and Davis, K.J.: Constraining the CO₂ budget of the corn belt: exploring uncertainties from the assumptions in a mesoscale inverse system, *Atmos. Chem. Phys.*, 12, 337–354, doi:10.5194/acp-12-337-2012, 2012.
- Lopez, M., Schmidt, M., Yver, C., Messenger, C., Worthy, D., Kazan, V., Ramonet, M., Bousquet, P., and Ciais, P.: Seasonal variation of N₂O emissions in France inferred from atmospheric N₂O and ²²²Rn measurements, *J. Geophys. Res.*, 117, D14103, doi: 10.1029/2012JD017703, 2012.
- 30 Lopez, M., Schmidt, M., Delmotte, M., Colomb, A., Gros, V., Janssen, C., Lehman, S. J., Mondelain, D., Perrussel, O., Ramonet, M., Xueref-Remy, I., and Bousquet, P.: CO, NO_x and ¹³CO₂ as tracers for fossil fuel CO₂: results from a pilot study in Paris during winter 2010, *Atmos. Chem. Phys.*, 13, 7343-7358, doi:10.5194/acp-13-7343-2013, 2013.

- Mac Kain, K., Wofsy, S. C., Nehrkorn, T., Eluszkiewicz, J., Ehleringer, J. R., and Stephens, B. B.: Assessment of ground-based atmospheric observations for verification of greenhouse gas emissions from an urban region, *PNAS*, 109 (22), 8423–8428, doi: 10.1073/pnas.1116645109, 2012.
- Mairie de Paris, Le Plan Climat de Paris, October 2007 (http://www.paris.fr/pratique/energie-plan-climat/le-plan-climat-de-paris/le-plan-climat-de-paris/rub_8413_stand_69591_port_19609)
- 5 Massen, F. and Beck, E.G.: Accurate estimation of CO₂ background level from near ground measurements at non-mixed environments. In: Filho WL (ed) *The economic, social and political elements of climate change*. *Climate Change Management* 509–522. doi:10.1007/978-3-642-14776-0_31, 2011.
- Menut, L., Flamant, C., Pelon, J., and Flamant, P. H.: Urban boundary layer height determination from lidar measurements
10 over the Paris area, *Appl. Opt.*, 38(6), 945–954, doi:10.1364/AO.38.000945, 1999.
- Messenger, C., Schmidt, M., Ramonet, M., Bousquet, P., Simmonds, P., Manning, A., Kazan, V., Spain, G., Jennings, S. G., and Ciais, P.: Ten years of CO₂, CH₄, CO and N₂O fluxes over Western Europe inferred from atmospheric measurements at Mace Head, Ireland, *Atmos. Chem. Phys. Discuss.*, 8, 1191–1237, doi:10.5194/acpd-8-1191-2008, 2008.
- Moriwaki, R., Kanda, M., and Nitta, H.: Carbon dioxide build-up within a suburban canopy layer in winter night, *Atmos.*
15 *Environ.* 40: 1394–1407, doi: 10.1016/j.atmosenv.2005.10.059, 2006.
- Nasrallah, H.A., Balling, Jr., R.C., Madi, S.M., and Al-Ansari, L.: Temporal variations in atmospheric CO₂ concentrations in Kuwait City, Kuwait with comparisons to Phoenix, Arizona, USA, *Environ. Poll.* 121, 301–305, doi: 0.1016/S0269-7491(02)00221-X, 2003.
- Newman, S., Xu, X., Affek, H. P., Stolper, E., and Epstein, S.: Changes in concentration and isotopic composition of CO₂ in
20 urban air from the Los Angeles basin, California, between 1972 and 2003, *J. Geophys. Res.*, 113, D23304, doi:10.1029/2008JD009999, 2008.
- Newman, S., Jeong, S., Fischer, M. L., Xu, X., Haman, C. L., Lefer, B., Alvarez, S., Rappenglueck, B., Kort, E. A., Andrews, A. E., Peischl, J., Gurney, K. R., Miller, C. E., and Yung, Y. L.: Diurnal tracking of anthropogenic CO₂ emissions in the Los Angeles basin megacity during spring 2010, *Atmos. Chem. Phys.*, 13, 4359–4372, doi:10.5194/acp-13-4359-2013,
25 2013.
- Pal, S., Xueref-Remy, I., Ammoura, L., Chazette, P., Gibert, F., Royer, P., Dieudonné, E., Dupont, J. C., Haeffelin, M., Lac, C., Lopez, M., Morille, Y., and Ravetta, F.: Spatio-temporal variability of the atmospheric boundary layer depth over the Paris agglomeration: An assessment of the impact of the urban heat island intensity, *Atmos. Env.*, 63, 261–275, doi:10.1016/j.atmosenv.2012.09.046, 2012.
- 30 Pataki, D. E., Emmi, P.C., Forster, C. B., Mills, J. I., Pardyjak, E. R., Peterson, T. R., Thompson, J. D., and Murphy, E. D.: An integrated approach to improving fossil fuel emissions scenarios with urban ecosystem studies, *Ecol. Complexity*, 6, 1–14, doi:10.1016/j.ecocom.2008.09.003, 2009.

- Pataki, D. E., Bowling, D. R., and Ehleringer, J. R.: Seasonal cycle of carbon dioxide and its isotopic composition in an urban atmosphere: Anthropogenic and biogenic effects, *J. Geophys. Res.*, 108 (D23), 4735, doi:10.1029/2003JD003865, 2003.
- Rella, C., Accurate Greenhouse Gas Measurements in Humid Gas Streams Using the Picarro G1301 Carbon Dioxide / Methane / Water Vapor Gas Analyzer, White Paper, PICARRO, 2010 (http://www.picarro.com/assets/docs/White_Paper_G1301_Water_Vapor_Correction.pdf).
- Rayner, P. J., Raupach, M.R., Paget, M., Peylin, P., and Koffi, E.: A new global gridded data set of CO₂ emissions from fossil fuel combustion: Methodology and evaluation, *J. Geophys. Res.*, 155 (D19), D19306, 10.1029/2009JD013439, 2010.
- Rice, A. and Bostrom, G.: Measurements of carbon dioxide in an Oregon metropolitan region, *Atmos. Environ.* 45, 1138-1144, doi: 10.1016/j.atmosenv.2010.11.026, 2011.
- Rigby, M., Toumias, R., Fisher, R., Lowry, D., and Nisbet, E.: First continuous measurements of CO₂ concentration in central London using a compact diffusion probe, *Atmos. Environ.* 42 (39), 8943–8953, doi: 10.1016/j.atmosenv.2008.06.040, 2008.
- Rosenzweig, C., Solecki, W., Hammer, S.A., and Mehrotra, S.: Cities lead the way in climate-change action, *Nature* 909, doi: 10.1038/467909a, 2010.
- Schmidt, M., Lopez, M., Yver Kwok, C., Messenger, C., Ramonet, M., Wastine, B., Vuillemin, C., Truong, F., Gal, B., Parmentier, E., Cloué, O., and Ciais, P.: High-precision quasi-continuous atmospheric greenhouse gas measurements at Trainou tower (Orléans forest, France), *Atmos. Meas. Tech.*, 7, 2283-2296, https://doi.org/10.5194/amt-7-2283-2014, 2014
- Seto, K. C. and Dhakal, S.: Chapter 12: Human Settlements, Infrastructure, and Spatial Planning, Tech. rep., USA, 2014.
- Strong, C., Stwertka, C., Bowling, D. R., Stephens, B. B., and Ehleringer, J. R.: Urban carbon dioxide cycles within the Salt Lake Valley: A multiple-box model validated by observations, *Journal of Geophysical Research*, Vol. 116, D15307, doi:10.1029/2011JD015693, 2011.
- Staufe, J., Broquet, G., Bréon, F.-M., Puygrenier, V., Chevallier, F., Xueref-Remy, I., Dieudonné, E., Lopez, M., Schmidt, M., Ramonet, M., Perrussel, O., Lac, C., Wu, L., and Ciais, P.: A first year-long estimate of the Paris region fossil fuel CO₂ emissions based on atmospheric inversion, submit. to *Atm. Chem. and Phys.*, 3 March 2016.
- Turnbull, J.C., Rayner, P.J., Miller, J.B., Naegler, T., Ciais, P., and Cozic, A., On the use of ¹⁴CO₂ as a tracer for fossil fuel CO₂: quantifying uncertainties using an atmospheric transport model, *J. Geophys. Res.*, 114, D22302, 2009.
- Turnbull, J.C., Sweeney, C., Karion, A., Newberger, T., Lehman, S. J., Tans, P. P., Davis, K. J., Lauvaux, T., Miles, N. L., Richardson, S. J., Cambaliza, M. O., Shepson, P. B., Gurney, K., Patarasuk, R., and Razlivanov, I.: Toward quantification and source sector identification of fossil fuel CO₂ emissions from an urban area: Results from the INFLUX experiment, *J. Geophys. Res. Atmos.*, 120, doi:10.1002/2014JD022555, 2015.
- United Nations, Department of Habitat, Hot Cities: battle-ground for Climate Change, Global report on human settlement 2011, 2011a.
- United Nations, Department of Economic and Social Affairs/ Population division: World Urbanization Prospects: The 2011 Revision, 2011b.

- Vogel, F. R., Hammer, S., Steinhof, A., Kromer, B., and Levin, I.: Implication of weekly and diurnal ^{14}C calibration on hourly estimates of CO-based fossil fuel CO_2 at a moderately polluted site in southwestern Germany, *Tellus B*, 62: 512–520. doi: 10.1111/j.1600-0889.2010.00477.x, 2010.
- Vermeulen, A. T., Hensen, A., Popa, M. E., van den Bulk, W. C. M., and Jongejan, P. A. C.: Greenhouse gas observations from Cabauw Tall Tower (1992–2010), *Atmos. Meas. Tech.*, 4, 617–644, doi: 10.5194/amt-4-617-2011, 2011.
- Wang, Y., Munger, J.W., Xu, S., McElroy, M.B., Hao, J., Nielsen, C.P., and Ma, H.: CO_2 and its correlation with CO at a rural site near Beijing: implications for combustion efficiency in China, *Atmos. Chem. Phys.*, 10, 8881–8897, doi: 10.5194/acp-10-8881-2010, 2010.
- Verhulst, K.R., Karion, A., Kim, J., Salameh, P.K., Keeling, R.F., Newman, S., Miller, J., Sloop, C., Pongetti, T., Rao, P., Wong, C., Hopkins, F., Yadav, V., Weiss, R.F., Duren, R.M., and Miller, C.E.: Carbon Dioxide and Methane Measurements from the Los Angeles Megacity Carbon Project: 1. Calibration, Urban Enhancements, and Uncertainty Estimates, *Atmos. Chem. Phys. Discuss.*, doi:10.5194/acp-2016-850, 2016, under review for ACP.
- Wentz, E. A., Gober, P., Balling, Jr., R. C., and Day, T.: Spatial patterns and determinants of carbon dioxide in an urban environment, *Ann. Assoc. Am. Geogr.*, 92, 15–28, doi: 10.1111/1467-8306.00277, 2002.
- Widory, D. and Javoy, M.: The carbon isotope composition of atmospheric CO_2 in Paris, *Earth and Planetary Science Letters* 215, 289–298, doi: 10.1016/S0012-821X(03)00397-2, 2003.
- Wolf, Jr., C., Dalal, S., DaVanzo, J., Larson, E. V., Akhmedjonov, A., Dogo, H., Huang, M., and Montoya, S.: China and India, 2025: a comparative assessment, RAND Corporation, 2011.
- Xueref-Remy, I., Dieudonné, E., Lopez, M., Vuillemin, C., Pal' S., Schmidt M., and Ampe, C.: Assessing Paris megacity CO_2 urban dome: analysis of 1 year of data from the CO_2 -Megaparis project (Aug.2010-Jul.2011), AGU Fall Meeting 2012, Abstract GC53B-1272, 2012.
- Xueref-Remy, I., Messenger, C., Filippi, D., Pastel, M., Nedelec, P., Ramonet, M., Paris, J. D., and Ciais, P.: Variability and budget of CO_2 in Europe: analysis of the CAATER airborne campaigns – Part 1: Observed variability, *Atmos. Chem. Phys.*, 11, 5655–5672, doi:10.5194/acp-11-5655-2011, 2011.
- Zhao, C. L. and Tans, P.P.: Estimating uncertainty of the WMO mole fraction scale for carbon dioxide in air, *J. Geophys. Res.-Atm.*, 111(D8), 10.1029/2005JD006003, 2006 (https://www.esrl.noaa.gov/gmd/ccl/co2_scale.html/).

Figure captions

Figure 1. Annual emissions of CO₂ from Île-de-France at a spatial resolution of 1x1 km² (AIRPARIF, 2010) and our Paris megacity CO₂ in-situ network: the red points indicate the CO₂-MEGAPARIS stations (MON = NE rural site, 9 m AGL, GON = NE peri-urban site, 4 m AGL and EIF = urban site, 317 m AGL); the dark blue points are stations from the ICOS-France network (GIF = SW peri-urban site, 7 m AGL, TRN = SW rural site, 50 & 180 m AGL). The QUALAIR station for monitoring the atmospheric boundary layer height in the Paris city is also shown (green point).

Figure 2. Location of the Paris megacity on a map of CO₂ anthropogenic emissions from Western Europe, adapted from the Edgar 2009 inventory (<http://edgar.jrc.ec.europa.eu/>, 2009). Emissions are given in Tg of CO₂-eq per grid cell (10 x 10 km²). Some of the main emitting points in Western Europe are also given. The geographical position of the remote site of Mace Head (MHD) on the west coast of Ireland is also shown.

Figure 3. Wind rose at GIF (7 m AGL, SW peri-urban site) given by season over the period of study (8 August 2010–13 July 2011) from the Meso-NH modeled wind fields. Colors indicate the wind speed according to the given scale (in m s⁻¹).

Figure 4a. Time series of CO₂ concentration (1 hour averages) recorded during the CO₂-Megaparis period and colored by wind classed for sites MON (NE rural site, 9 m AGL), GON (peri-urban site, 4 m AGL), EIF (urban site, 317 m AGL) and GIF (SW peri-urban site, 7 m AGL).

Figure 4b. Time series of CO₂ concentration (1 hour averages) recorded during the CO₂-Megaparis period and colored by wind classed for sites TRN50 (rural SW, 50 m AGL) and MHD (coastal remote site, 15 m AGL).

Figure 5 (a to d'). Left: Diurnal cycles of CO₂ from 1 h averages at (a) MON (NE rural site, 9 m AGL), (b) GON (NE peri-urban site, 4 m AGL), (c) EIF (urban site, 317 m AGL) and (d) GIF (SW peri-urban site, 7 m AGL). Right: Diurnal cycles of CO₂ by season at (a') MON, (b') GON, (c') EIF and (d') GIF. Note that the left and right plot scales are not the same.

Figure 5 (e to g'). Left: Diurnal cycles of CO₂ from 1 h averages at: (e) TRN50 (SW rural site, 50 m AGL), (f) TRN180 (SW rural site, 180 m AGL) and (g) MHD (remote site, 15 m AGL). Right: Diurnal cycles of CO₂ by season at: (e') TRN50, (f') TRN180 and (g') MHD. Note that the left and right plot scales are not the same.

Figure 6. Diurnal cycles of the hourly LBLH (Lower BLH) estimate means (in black) $\pm 1-\sigma$ standard deviation (in grey) and of the CO₂ hourly means (in red) observed by season at QUALAIR (urban site, 25 m AGL) and EIF (urban site, 317 m AGL), respectively. Time is in hour UTC. The blue horizontal line is the elevation of EIF. The violet circles give the CO₂ concentration (according to the red scale) at the same moments when the LBLH (in black) was measured.

- 5 Figure 7. Left: CO₂ diurnal cycle by day of the week at the different stations, calculated from CO₂ hourly concentrations over the whole period of study. Right: standard variation ($1-\sigma$) of the hourly CO₂ mean concentration.

Figure 8a. Seasonal cycles of CO₂ concentration at the six sites based on monthly means. Monthly averages of air temperature at 100 m (Saclay tower near GIF) and of the LBLH (QUALAIR urban site, 25 m AGL) are also shown. Memo (in m AGL) : MON = 9 m (NE rural site), GON = 4 m (NE peri-urban site), EIF = 317 m (urban site), GIF = 7 m (SW peri-urban site), TRN50 = 50 m (SW rural site), TRN180 = 180 m (SW rural site), MHD = 15 m (remote site).

Figure 8b. Seasonal cycle (Aug.2010-Jul.2011) of CO₂ at each of the Paris regional sites and at MHD, calculated from CO₂ monthly means of hourly averages, with error bars showing one standard deviation ($\pm 1-\sigma$) of the CO₂ means. Memo (in m AGL) : MON = 9 m (NE rural site), GON = 4 m (NE peri-urban site), EIF = 317 m (urban site), GIF = 7 m (SW peri-urban site), TRN50 = 50 m (SW rural site), TRN180 = 180 m (SW rural site), MHD = 15 m (remote site).

- 15 Figure 9. Left: Hourly means of the CO₂ concentration recorded at GON (NE peri-urban site, 4 m AGL) as a function of wind speed and colored by wind direction (the color scale is in degrees). Right: same for the CO₂ standard deviation ($1-\sigma$ of the hourly CO₂ concentration means).

Figure 10. Mean CO₂ concentration (in ppm) observed at the different stations of the Paris regional network (TRN represents the measurements at 50 m AGL) and at MHD for wind speed higher than 9 m s⁻¹ over the period of study (8 August 2010–13 July 2011). During such events, the synoptic conditions were mostly oceanic (wind blowing from the SW sector). Memo (in m AGL) : MON = 9 m (NE rural site), GON = 4 m (NE peri-urban site), EIF = 317 m (urban site), GIF = 7 m (SW peri-urban site), TRN50 = 50 m (SW rural site), TRN180 = 180 m (SW rural site), MHD = 15 m (remote site).

Figure 11. Left: CO₂ mean concentration as a function of wind speed (circles in m s⁻¹) and wind direction at MON (NE rural), GON (NE peri-urban), EIF (urban), GIF (SW peri-urban) and TRN50 (rural) stations using daytime data (11-15 h UTC) for the period of study (4 Aug.2010-11 July 2011). Middle: mean $1-\sigma$ CO₂ variability of each concentration (ws, wd) point. Right: occurrence as the frequency of the (ws, wd) bin weighted by the square-root of the CO₂ concentration mean.

Tables

Table 1. Coordinates of the stations used in this study (ASL stands for Above Sea Level; AGL for Above Ground Level).

Station	Code	Latitude (°)	Longitude (°)	Site ground elevation ASL	Sampling height AGL
Montgé-en-Goële	MON	49°01'41.79'' N	2°44'55.54'' E	160 m	9 m
Gonesse	GON	48°59'24.56'' N	2°27'21.90'' E	68 m	4 m
Eiffel tower	EIF	48°51'29.71'' N	2°17'39.92'' E	33 m	317 m
Gif-sur-Yvette	GIF	48°42'35.82'' N	2°08'51.55'' E	163 m	7 m
Traînou	TRN	47°57'53.08'' N	2°06'45.42'' E	133 m	50 m , 180m
Mace Head	MHD	53°19'33.00'' N	9°54'12.00'' W	25 m	15 m
QUALAIR	QUA	48°50'47.26'' N	2°21'21.40'' E	35 m	25 m

5

10

Table 2. Calibration and target frequencies, accuracy and repeatability of the CO₂-Megaparis stations. The accuracy is given as the difference of the target CO₂ concentrations measured by the CRDS analyzer and by the GC.

	EIF	MON	GON
Calibration sequence	2 h every 3 months	6 h every 2 weeks	6 h every 2 weeks
Target sequence	30 mn every 2 weeks	30 mn every 12 h	30 mn every 12 h
Accuracy (ppm)	0.13	-0.04	-0.07
Repeatability (ppm)	0.38	0.10	0.07

Table 3 Monthly means and standard deviation ($\pm 1-\sigma$) of the CO₂ concentration (in ppm) measured at each site and data coverage of each month (Coverage, in percent).

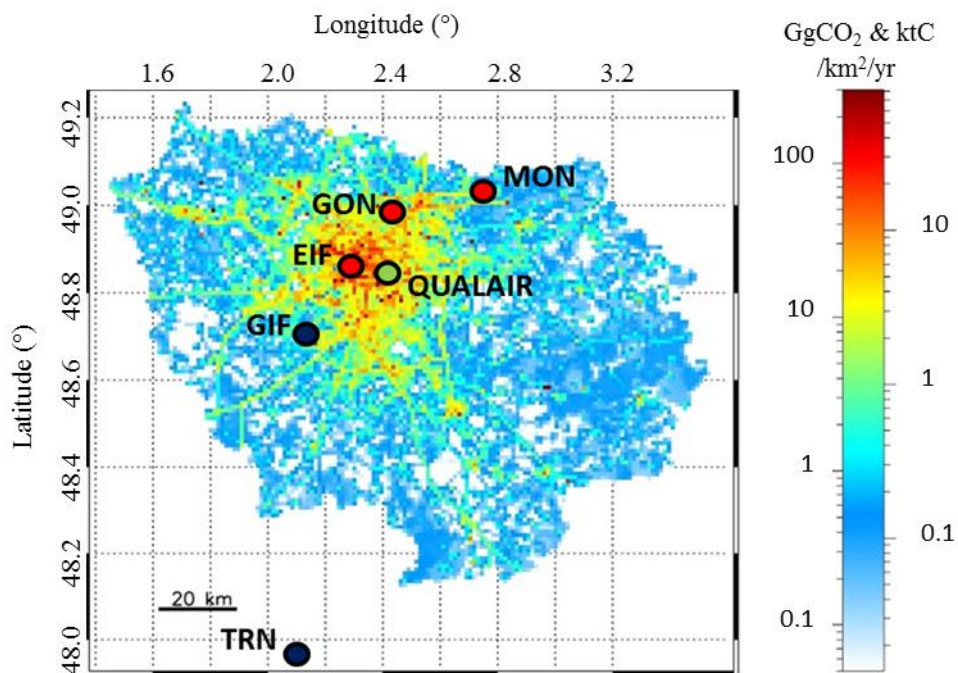
	MON	GON	EIF	GIF	TRN50	TRN180	MHD
Spring							
March	410.4±9.4	420.3±19.1	411.8 ±16.7	414.4±13.7	408.9±9.3	405.5±7.9	398.6±4.4
Coverage	99.9	97.3	95.6	93.0	57.7	66.8	87.6
April	402.1±11.0	421.2±32.6	403.0±13.2	408.7±15.3	401.3±11.2	396.8±7.1	398.6±4.9
Coverage	100.0	95.3	94.6	94.2	69.0	79.6	77.6
May	394.7±8.9	405.5±20.0	398.0±10.6	398.7±11.2	395.0±9.9	391.2±5.9	396.3±2.4
Coverage	99.9	97.3	98.8	98.3	81.2	82.8	95.6
Summer							
June	400.1±11.9	406.2±27.3	396.9±8.2	400.9±12.8	398.4±10.7	394.5±4.7	394.5±3.5
Coverage	98.1	0.65	95.3	84.9	88.2	69.3	92.9
July	393.1±6.9	398.6±17.3	393.4±6.6	397.2±8.3	392.4±6.2	389.8±3.2	392.1±5.0
Coverage	96.8	96.8	78.1	62.4	51.4	78.1	97.1

August	390.8±10.2	401.9±29.6	387.1± 7.9	392.2±11.8	389.8±10.8	384.9±5.6	381.4±2.5
Coverage	99.6	94.6	90.5	78.6	95.8	96.1	99.9
Autumn							
September	395.3±12.7	410.9±34.0	391.0±11.1	395.3±11.1	392.5±11.8	385.7±5.7	384.0±3.3
Coverage	72.9	96.0	97.8	83.1	91.1	90.4	96.8
October	402.8±9.8	413.9±24.7	400.8±12.0	403.0±11.3	400.3±10.6	395.0±7.2	390.9±6.2
Coverage	100.0	96.0	98.9	82.7	92.5	90.5	98.7
November	408.3±10.4	414.9±15.9	407.7±15.1	411.2±12.9	401.8±9.4	399.3±8.6	393.6±3.8
Coverage	100.0	97.2	99.6	67.4	34.3	31.5	97.1
Winter							
December	417.0±13.9	424.5±17.9	414.2±16.9	415.4±13.9	408.3±9.5	406.0±10.4	396.8±3.8
Coverage	100.0	73.9	71.9	77.4	82.4	87.5	97.2
January	408.9±9.4	415.8±16.7	408.4±13.2	410.1±13.0	405.7±10.1	403.1±9.3	396.1±2.3
Coverage	100.0	96.2	78.9	78.5	95.6	94.5	98.7
February	411.9±12.2	423.1±20.7	410.5±14.7	409.8±10.5	405.4±7.8	402.8±7.3	396.3±2.0
Coverage	100.0	97.0	93.2	97.0	84.8	88.5	98.4

Table 4. Mean altitude of the lowest estimate of the boundary layer height (LBLH) by season in the morning and early afternoon (hours are given UTC, altitude in meters AGL). The number of points used to calculate the means are also given (N).

Time (UTC)	5 h	6 h	7 h	8 h	9 h	10 h	11 h	12 h	13 h
Spring									
LBLH	NaN	410	442	520	593	697	833	899	935
N	0	9	11	11	12	12	12	13	13
Summer									
LBLH	513	583	728	992	1178	1324	1400	1405	1531
N	7	13	13	13	13	13	11	11	7
Autumn									
LBLH	351	394	451	615	751	837	896	947	940
N	16	25	31	34	33	33	33	31	30
Winter									
LBLH	NaN	301	349	384	419	440	470	516	550
N	0	3	15	24	23	25	26	27	29

Figures

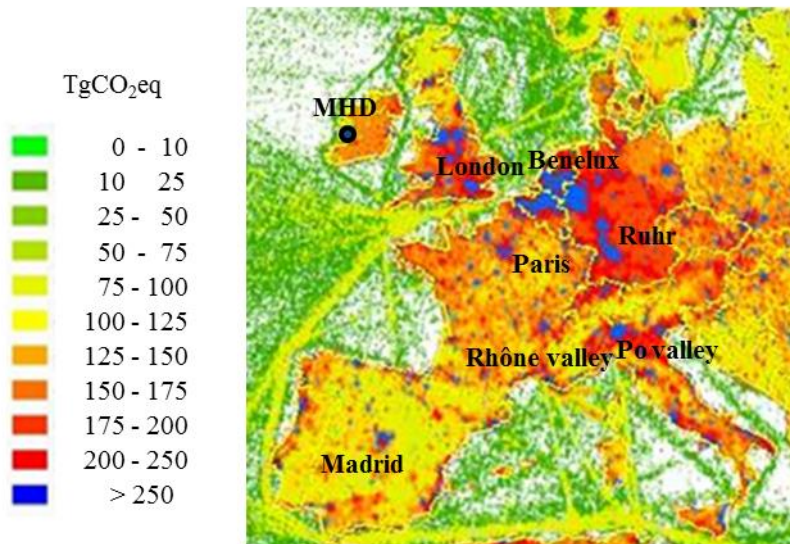


5

Figure 1. Annual emissions of CO₂ from Île-de-France at a spatial resolution of 1x1 km² (AIRPARIF, 2010) and our Paris megacity CO₂ in-situ network: the red points indicate the CO₂-MEGAPARIS stations (MON = NE rural site, 9 m AGL, GON = NE peri-urban site, 4 m AGL and EIF = urban site, 317 m AGL); the dark blue points are stations from the ICOS-France network (GIF = SW peri-urban site, 7 m AGL, TRN = SW rural site, 50 & 180 m AGL). The QUALAIR station for monitoring the atmospheric boundary layer height in the Paris city is also shown (green point).

10

15



5

Figure 2. Location of the Paris megacity on a map of CO₂ anthropogenic emissions from Western Europe, adapted from the Edgar 2009 inventory (<http://edgar.jrc.ec.europa.eu/>, 2009). Emissions are given in Tg of CO₂-eq per grid cell (10 x 10 km²). Some of the main emitting points in Western Europe are also given. The geographical position of the remote site of Mace Head (MHD) on the west coast of Ireland is also shown.

10

15

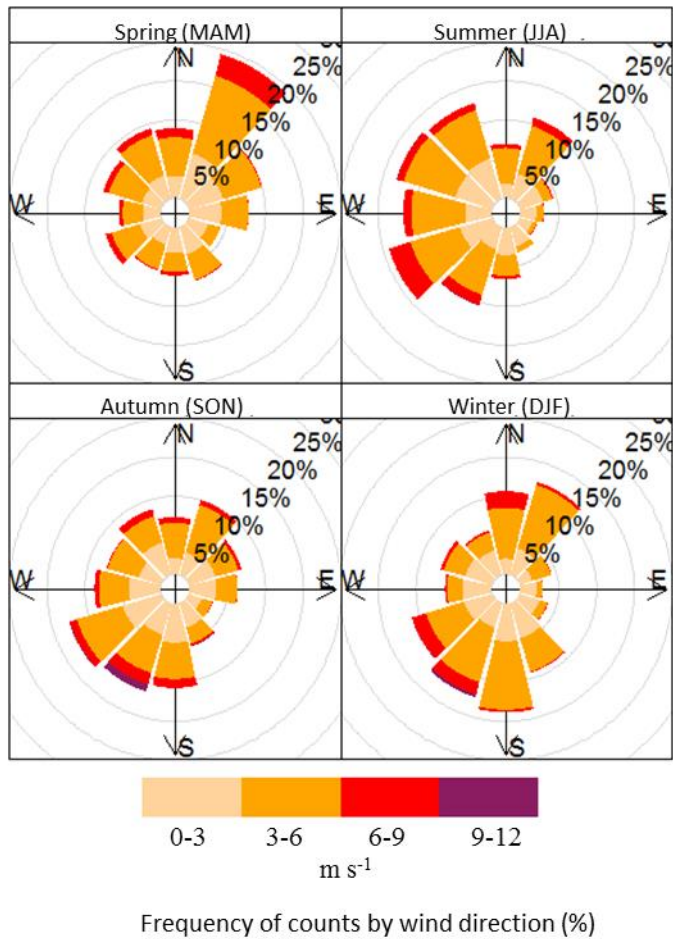


Figure 3. Wind rose at GIF (7 m AGL, SW peri-urban site) given by season over the period of study (8 August 2010–13 July 2011) from the Meso-NH modeled wind fields. Colors indicate the wind speed according to the given scale (in m s^{-1}).

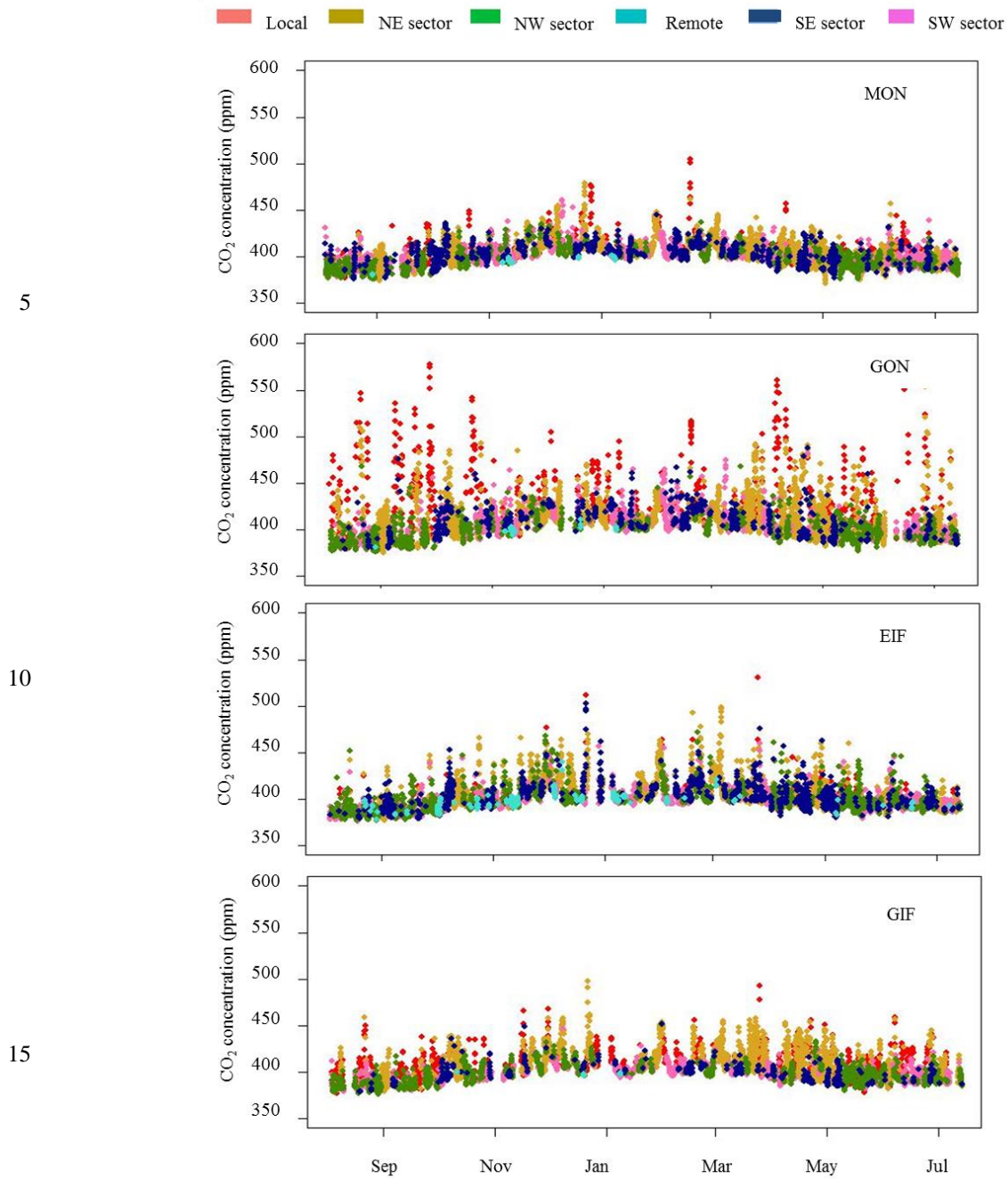
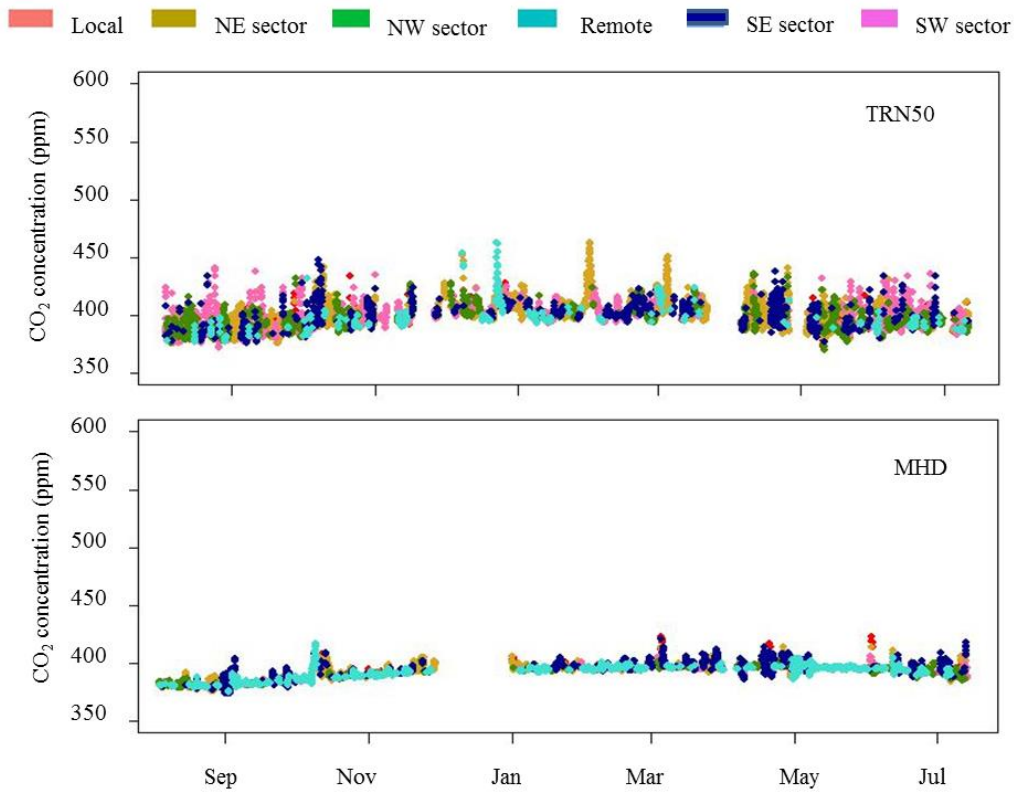


Figure 4a. Time series of CO₂ concentration (1 hour averages) recorded during the CO₂-Megaparis period and colored by wind classed for sites MON (NE rural site, 9 m AGL), GON (peri-urban site, 4 m AGL), EIF (urban site, 317 m AGL) and GIF (SW peri-urban site, 7 m AGL).

5



10

Figure 4b. Time series of CO₂ concentration (1 hour averages) recorded during the CO₂-Megaparis period and colored by wind classed for sites TRN50 (rural SW, 50 m AGL) and MHD (coastal remote site, 15 m AGL).

15

20

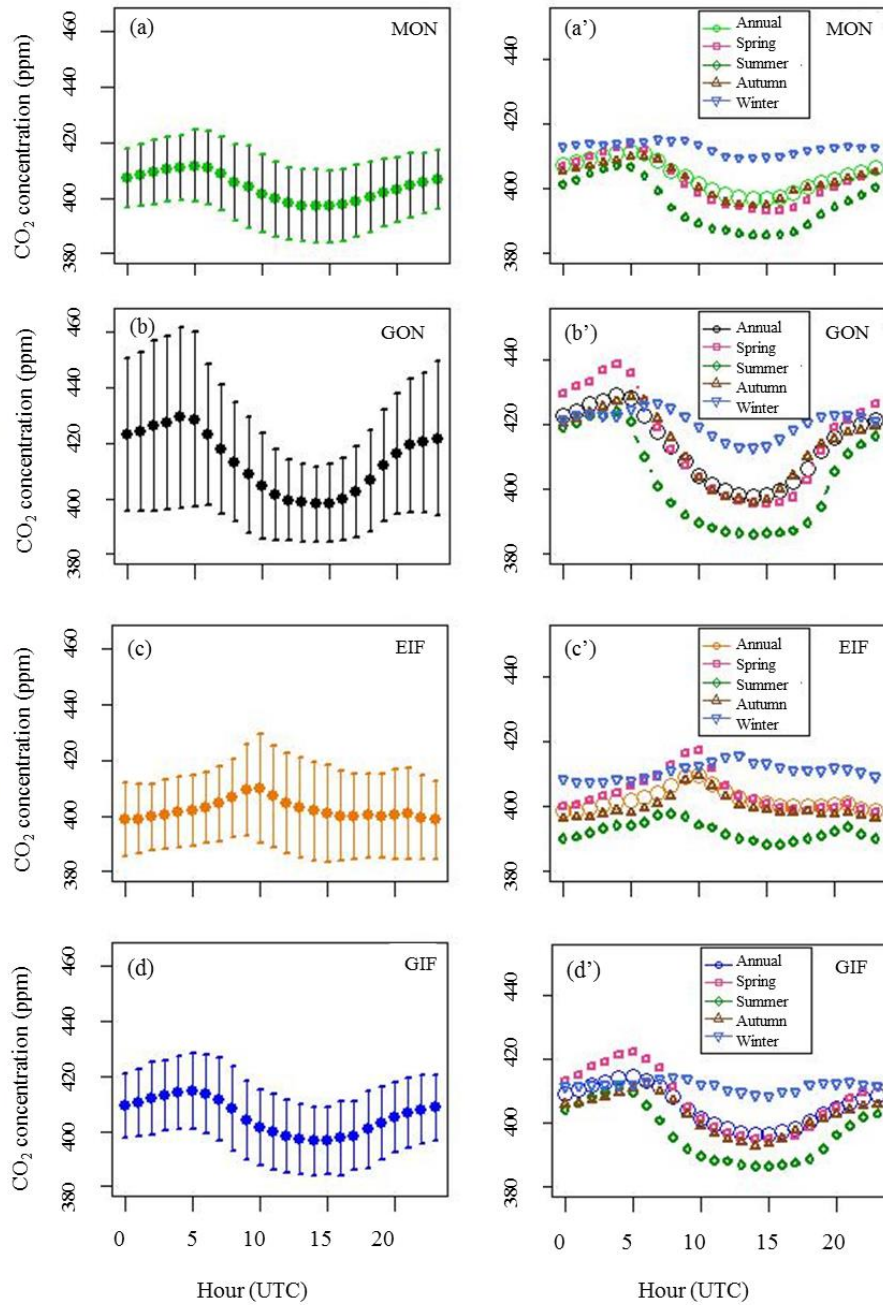


Figure 5 (a to d'). Left: Diurnal cycles of CO₂ from 1 h averages at (a) MON (NE rural site, 9 m AGL), (b) GON (NE peri-urban site, 4 m AGL), (c) EIF (urban site, 317 m AGL) and (d) GIF (SW peri-urban site, 7 m AGL). Right: Diurnal cycles of CO₂ by season at (a') MON, (b') GON, (c') EIF and (d') GIF. Note that the left and right plot scales are not the same.

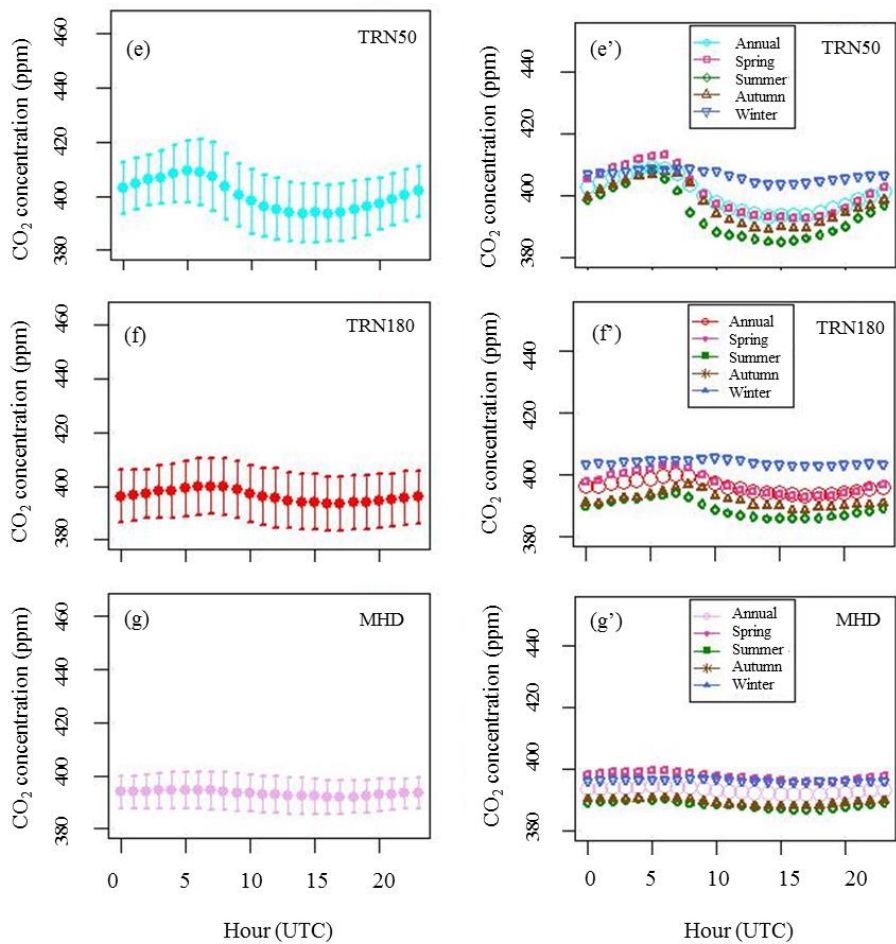


Figure 5 (e to g'). Left: Diurnal cycles of CO₂ from 1 h averages at: (e) TRN50 (SW rural site, 50 m AGL), (f) TRN180 (SW rural site, 180 m AGL) and (g) MHD (remote site, 15 m AGL). Right: Diurnal cycles of CO₂ by season at: (e') TRN50, (f') TRN180 and (g') MHD. Note that the left and right plot scales are not the same.

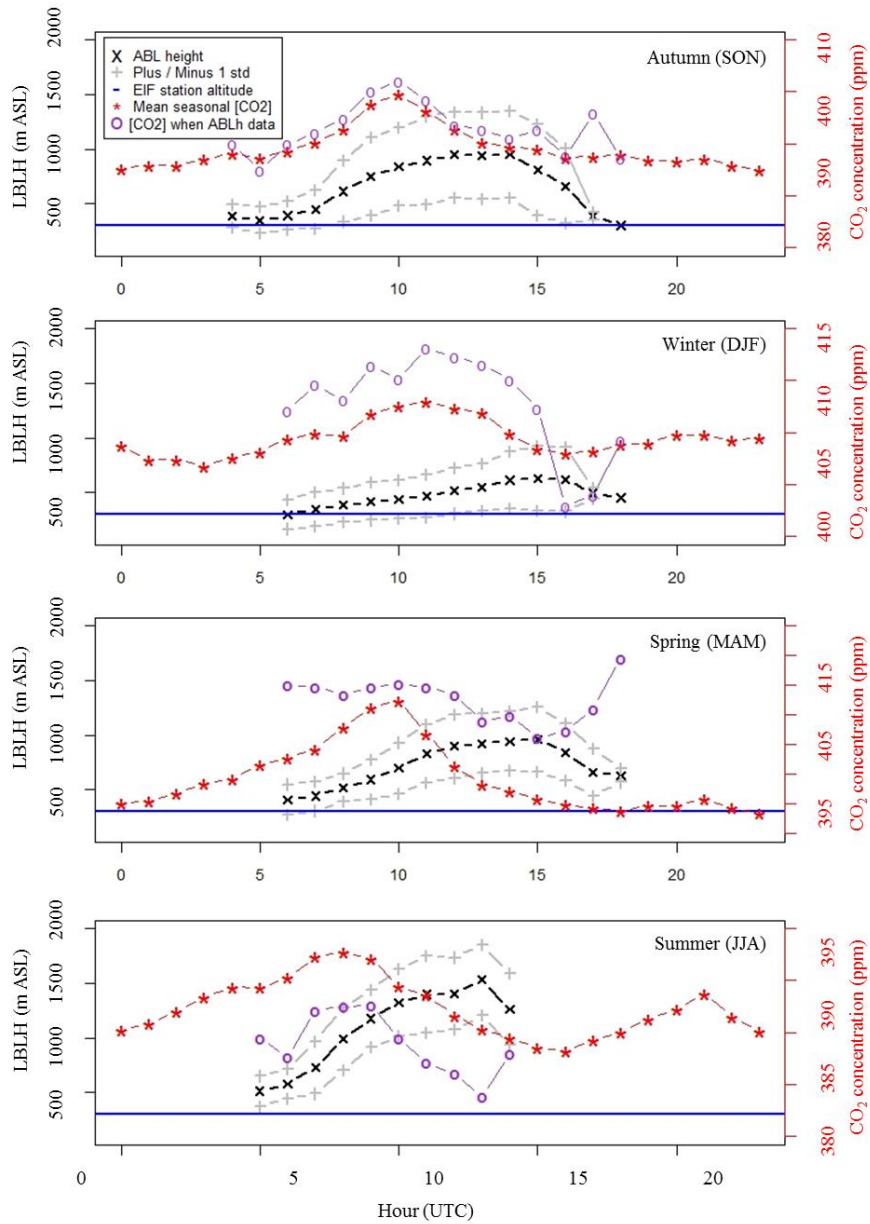
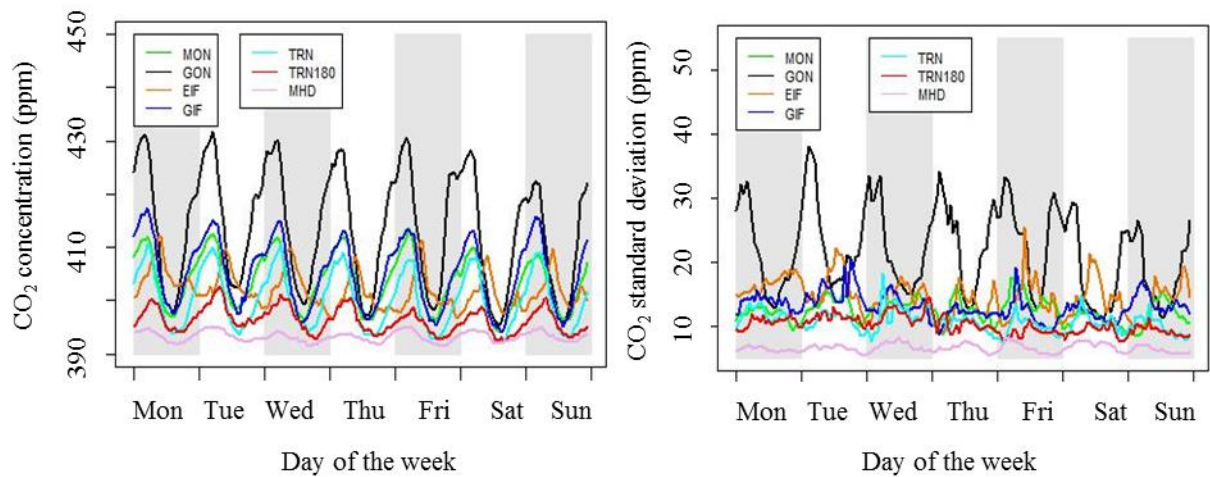


Figure 6. Diurnal cycles of the hourly LBLH (Lower BLH) estimate means (in black) $\pm 1\text{-}\sigma$ standard deviation (in grey) and of the CO₂ hourly means (in red) observed by season at QUALAIR (urban site, 25 m AGL) and EIF (urban site, 317 m AGL), respectively. Time is in hour UTC. The blue horizontal line is the elevation of EIF. The violet circles give the CO₂ concentration (according to the red scale) at the same moments when the LBLH (in black) was measured.

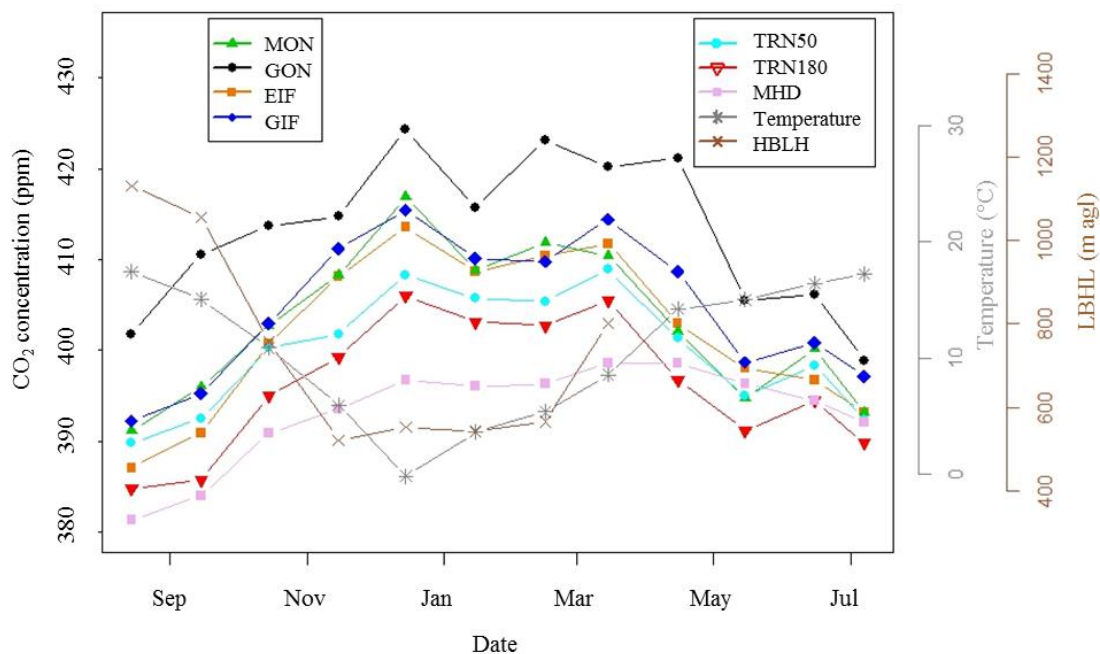


5

Figure 7. Left: CO₂ diurnal cycle by day of the week at the different stations, calculated from CO₂ hourly concentrations over the whole period of study. Right: standard variation ($1-\sigma$) of the hourly CO₂ mean concentration.

10

15



5 Figure 8a. Seasonal cycles of CO₂ concentration at the six sites based on monthly means. Monthly averages of air temperature at 100 m (Saclay tower near GIF) and of the LBLH (QUALAIR urban site, 25 m AGL) are also shown. Memo (in m AGL) : MON = 9 m (NE rural site), GON = 4 m (NE peri-urban site), EIF = 317 m (urban site), GIF = 7 m (SW peri-urban site), TRN50 = 50 m (SW rural site), TRN180 = 180 m (SW rural site), MHD = 15 m (remote site).

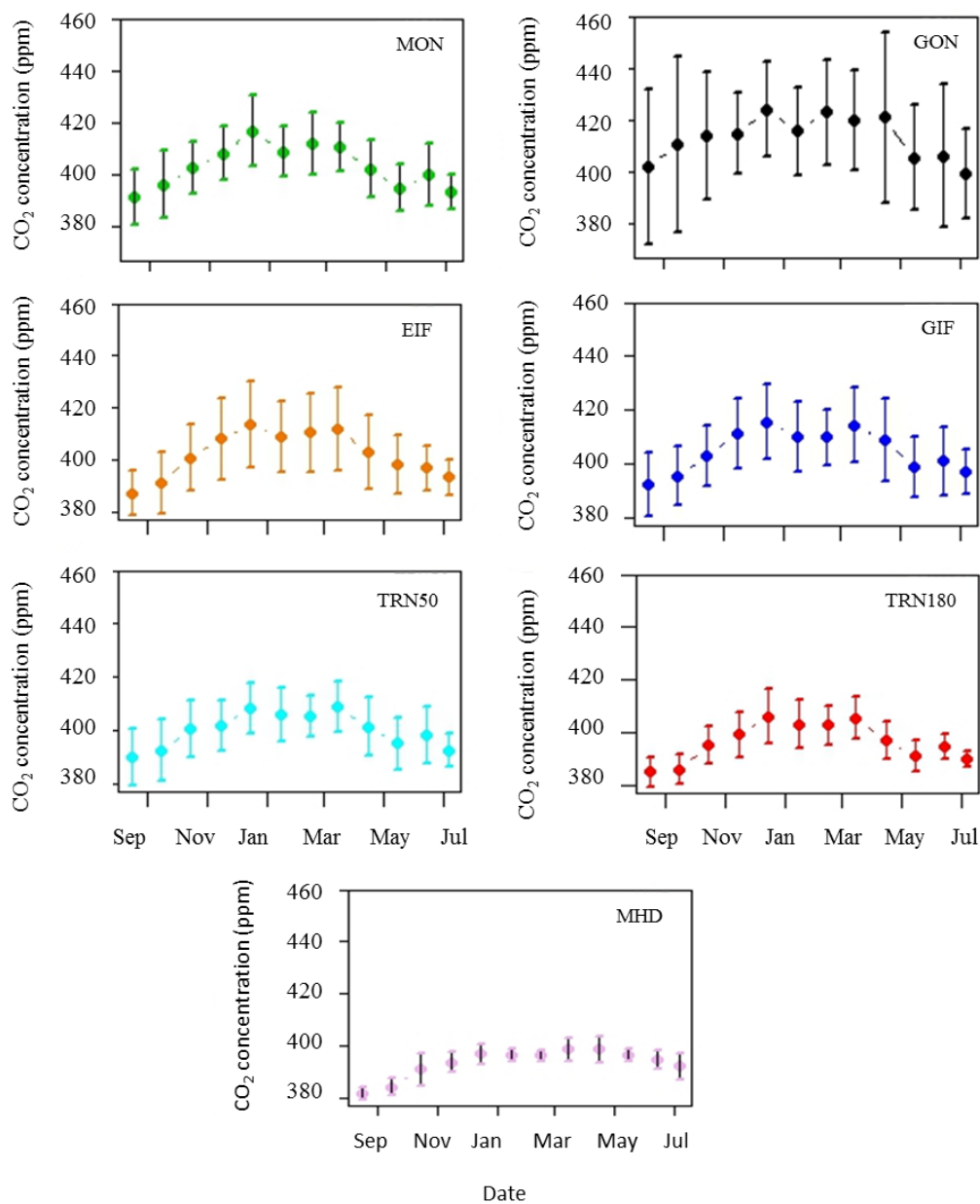
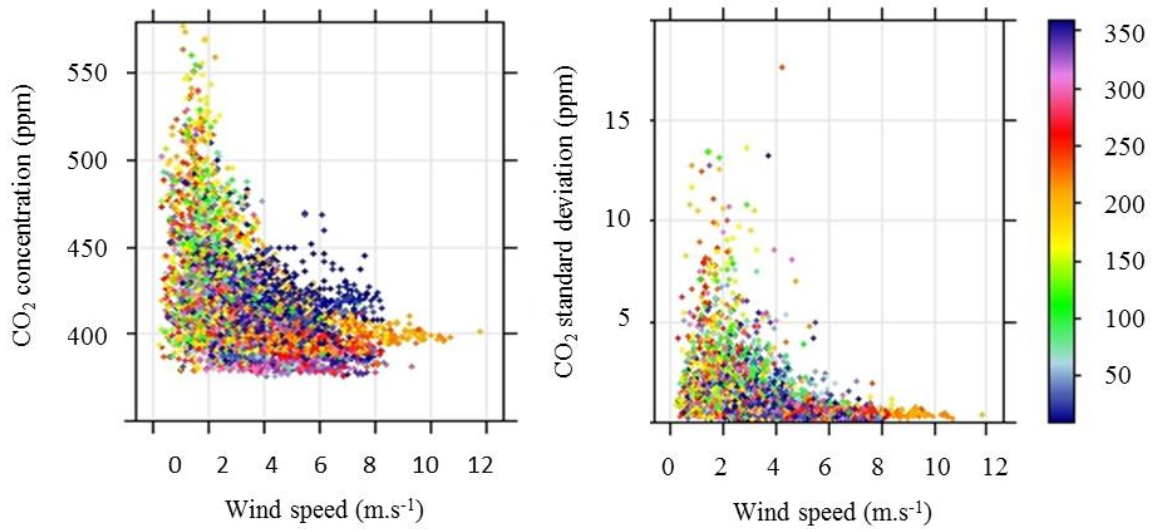


Figure 8b. Seasonal cycle (Aug.2010-Jul.2011) of CO₂ at each of the Paris regional sites and at MHD, calculated from CO₂ monthly means of hourly averages, with error bars showing one standard deviation ($\pm 1-\sigma$) of the CO₂ means. Memo (in m AGL) : MON = 9 m (NE rural site), GON = 4 m (NE peri-urban site), EIF = 317 m (urban site), GIF = 7 m (SW peri-urban site), TRN50 = 50 m (SW rural site), TRN180 = 180 m (SW rural site), MHD = 15 m (remote site).



5

Figure 9. Left: Hourly means of the CO₂ concentration recorded at GON (NE peri-urban site, 4 m AGL) as a function of wind speed and colored by wind direction (the color scale is in degrees). Right: same for the CO₂ standard deviation (1- σ of the hourly CO₂ concentration means).

10

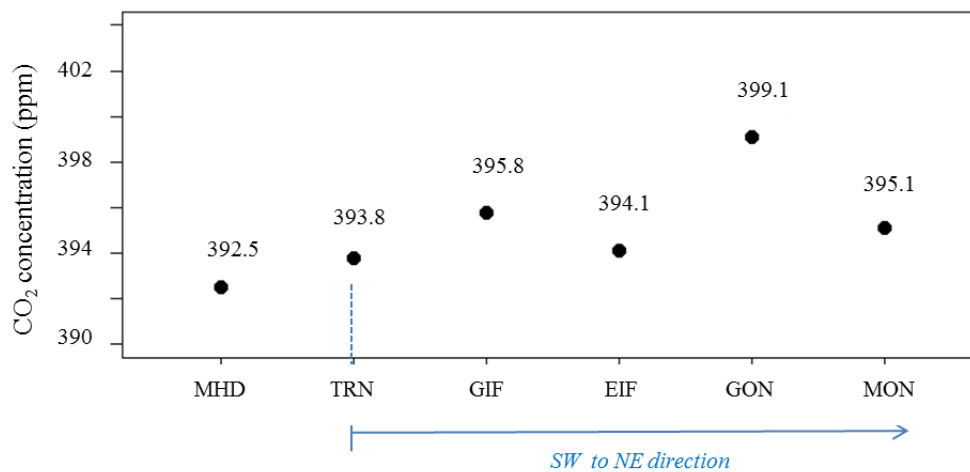


Figure 10. Mean CO₂ concentration (in ppm) observed at the different stations of the Paris regional network (TRN represents the measurements at 50 m AGL) and at MHD for wind speed higher than 9 m s⁻¹ over the period of study (8 August 2010–13 July 2011). During such events, the synoptic conditions were mostly oceanic (wind blowing from the SW sector). Memo (in m AGL) : MON = 9 m (NE rural site), GON = 4 m (NE peri-urban site), EIF = 317 m (urban site), GIF = 7 m (SW peri-urban site), TRN50 = 50 m (SW rural site), TRN180 = 180 m (SW rural site), MHD = 15 m (remote site).

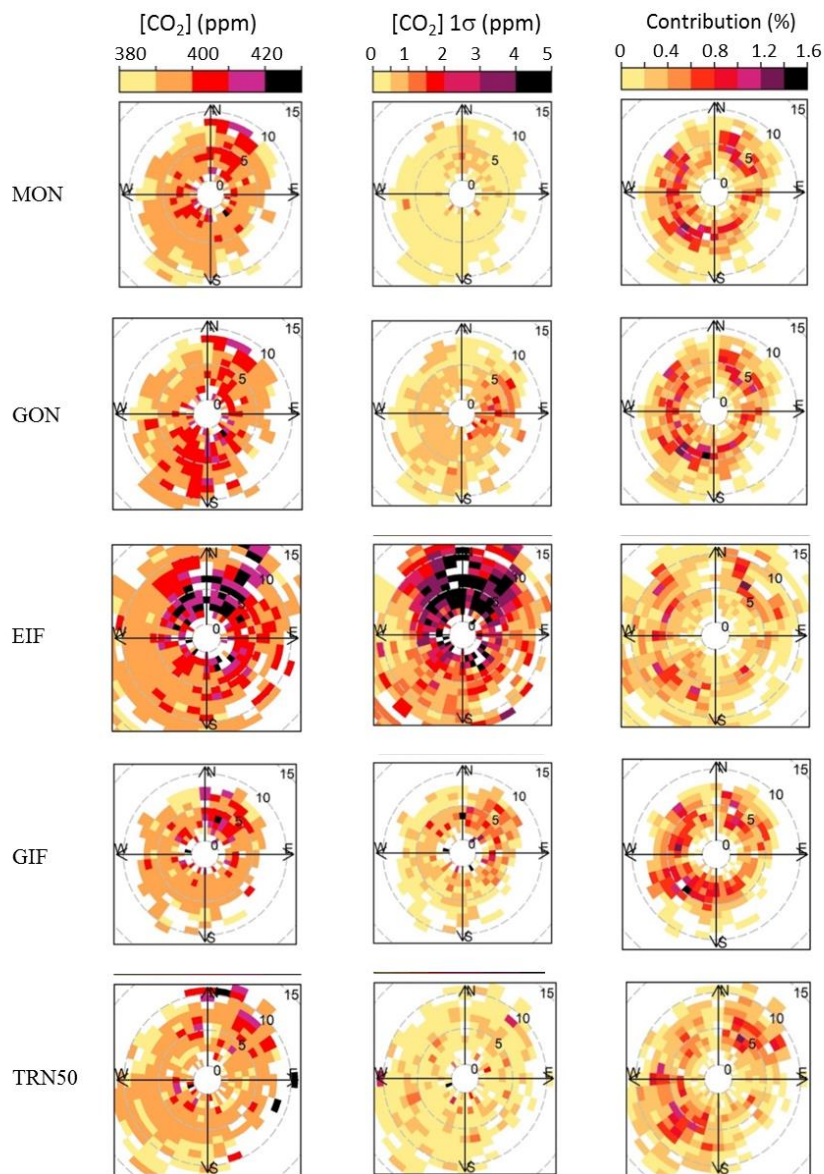


Figure 11. Left: CO₂ mean concentration as a function of wind speed (circles in m s⁻¹) and wind direction at MON (NE rural), GON (NE peri-urban), EIF (urban), GIF (SW peri-urban) and TRN50 (rural) stations using daytime data (11-15 h UTC) for the period of study (4 Aug.2010-11 July 2011). Middle: mean 1-σ CO₂ variability of each concentration (ws, wd) point. Right: occurrence as the frequency of the (ws, wd) bin weighted by the square-root of the CO₂ concentration mean.